Invasive macroalgae shape chemical and microbial waterscapes on coral reefs

Check for updates

Chloé Pozas-Schacre [1] ✉, Hugo Bischoff[2], Delphine Raviglione [1,3], Slimane Chaib[1],
Camille Clerissi [1,4], Isabelle Bonnard[1,3,4] & M. Nugues Maggy [1,4]

Over the past decades, human impacts have changed the structure of tropical benthic reef communities towards coral depletion and macroalgal proliferation. However, how these changes have modified chemical and microbial waterscapes is poorly known. Here, we assessed how the experimental removal of macroalgal assemblages influences the chemical and microbial composition of two reef boundary layers, the benthic and the momentum. Chemical and microbial waterscapes were spatially structured, both horizontally and vertically, according to macroalgal dominance and boundary layers. Microbes associated with reef degradation were enriched in the boundary layers surrounding macroalgal-dominated substrata. Dominant macroalgae were surrounded by a distinct chemical pool of diverse lipid classes (e.g., diterpenoids and glycerolipids) and labile organic matter (e.g., organooxygen compounds), which diffused from algal tissues to boundary layers according to their polarity. Finally, our results highlighted strong co-variations between specific algal-derived metabolites and planktonic microbes, giving insight into their roles in coral reef functioning and resilience.

Coral reefs are among the most productive and diverse ecosystems on the planet. Their high productivity in oligotrophic tropical seas depends on a tight benthic-pelagic coupling and key microbial processes[1–3]. Benthic organisms, like stony corals, macroalgae, or turf, release an extensive amount of dissolved and particulate organic matter underpinning reef community metabolism. For example, photosynthates and coral mucus constitute labile organic matter consumed by microbial assemblages tunneling essential nutrients through the coral reef food web[1,4,5]. Part of this chemical diversity can act as powerful cues involved in communication or defense structuring reef communities[6,7]. As such, the chemical pool in which sessile organisms bathe mediates both positive (e.g., settlement cues, metabolites exchange) and negative (e.g., allelopathy, competition) biotic interactions between reef members[6,8]. The combination of molecular exchanges and microbial processes within reef waters results in complex chemical and microbial waterscapes which are just starting to be deciphered[9–11].

Water masses of variable thickness emerge from drag forces as water flows over the reef geomorphology, resulting in a physical stratification of reef waterscapes[12]. Three boundary layers have been described: the benthic boundary layer (BBL—m to cm scale) influenced by the overall shape of the reef and main currents; the momentum boundary layer (MBL—cm to mm scale) receiving organic matter from the benthos through advection; and the diffusive boundary layer (DBL—mm to μm scale) essentially formed by the diffusion and accumulation of benthic products[12]. These water masses are dynamic, influenced by flow velocity and benthos complexity, causing variation in the transfer of organic matter within and between boundary layers[13]. Therefore, each boundary layer may have distinct biological and chemical characteristics, reflecting both benthic member identities and physical processes.

Accumulating anthropogenic pressures, such as ocean warming, pollution and overuse, have drastically altered the sessile community structure of the reef benthos, inducing phase shifts from coral to macroalgal dominance with cascading effects down to microbial scale[14,15]. Large-scale studies, across reefs and ocean basins, have demonstrated that the pelagic microbiome reflects the underlying benthos of shifted reefs. Specifically, reefs that have transitioned towards macroalgal dominance tend to harbor higher microbial density and abundance of copiotrophic, potentially pathogenic, microbial taxa than coral-dominated reefs[14,16,17]. Reef taxa actually exert a strong organismal influence on microbial assemblages, although limited to their immediate vicinity. Benthic primary producers, such as corals, macroalgae or turf algae, exhibit highly distinct microbial assemblages in their MBLs, which also differ from those of the upper water layer[10,18]. These microbial shifts are likely driven by concurrent changes in benthic-derived organic matter, yet its composition and small-scale spatial

[1]PSL Université Paris: EPHE-UPVD-CNRS, UAR 3278 CRIOBE, Université de Perpignan, Perpignan, France. [2]PSL Université Paris: EPHE-UPVD-CNRS, UAR 3278 CRIOBE BP 1013, Papeto'ai, Mo'orea, French Polynesia. [3]Plateau MSXM plateforme Bio2Mar, Université de Perpignan, Perpignan, France. [4]Laboratoire d'Excellence "CORAIL", Perpignan, France. ✉e-mail: pozaschloe@gmail.com

variation across boundary layers and benthic organisms remain inadequately understood.

In the last two decades, several studies have provided essential groundwork for unveiling the differential influence of benthic communities on chemical diversity and the link with microbial processes[4,19–22]. Coral and macroalgal exudates have specific chemical signatures and select for taxonomically and functionally distinct microbial communities. Specifically, carbon-rich algal exudates select for copiotrophic bacteria with more potential virulence factors compared to coral exudates[4]. Yet, it is only recently, with the advancement in marine untargeted metabolomics and chemoinformatics[23–26], that these metabolite pools have been shown to differ in their elemental stoichiometry and macronutrient content[21]. However, in-situ investigations of the chemical composition of reef waters, as well as their sources, remain scarce[9,11,27]. For example, molecular gradients from coral surface to overlying boundary layers have been described, comprising infochemicals, such as quorum sensing and antibacterial compounds, that may structure microbial communities surrounding the coral holobiont[27]. Conversely, in two recent studies, untargeted chemical composition of reef exometabolomes did not vary across depths[9] and did not reflect benthic composition across habitats[11].

Linking changes in metabolite pools and microbiome structure induced by macroalgal dominance is paramount to understand the ecology of transitioning reefs. Dominance of macroalgae may alter reef biogeochemical cycles through changes in microbe-metabolite interactions[1,14]. Additionally, water-mediated effects involving waterborne allelochemicals and microbially-mediated processes are thought to be involved in coral-algal competition[6,28,29]. If algal-associated microbial and chemical waterscapes drive the demise of coral reefs, they could create a feedback loop that reinforces macroalgal dominance[28]. In the light of accelerating coral reef degradation, a better comprehension of the effects of macroalgal assemblages on chemical and microbial signatures across reef boundary layers, as well as the origin and diffusion of algal-derived metabolites, is needed.

Here we describe an in-situ manipulative experiment in the lagoon of Mo'orea, French Polynesia, designed to assess how macroalgal assemblages influence the chemical and microbial composition of two reef boundary layers: the MBL and BBL. We sampled reef waters surrounding algal-dominated and algal-removed coral bommies and investigated algal-derived metabolites and microbes using untargeted metabolomics tandem mass spectrometry (LC-MS/MS) and 16S rDNA metabarcoding. Our integrative analysis reveals a spatial structuring of the chemical and microbial waterscapes according to macroalgal dominance and boundary layers, with an enrichment of opportunist copiotrophic bacteria in algal-associated waters. By investigating compound class identities in two invasive macroalgae and their associated boundary layers, we also show diffusion gradients of distinct compound classes and highlight co-variations between algal-derived metabolites and planktonic microbes.

Results

Experimental design overview and benthic community composition

This in-situ experiment took place in the lagoon of Mo'orea, French Polynesia, between June 2020 and June 2021 (Supplementary Fig. 1a). Six coral bommies were randomly selected and assigned to one of two algal treatments: (i) algal-removed or (ii) algal-dominated (Fig. 1a, b; Supplementary Fig. 1b). Algal-removed bommies were created by removal of all macroalgae. Macroalgal-dominated bommies were left untouched. Before algal removal, benthic communities did not differ between treatments (PERMANOVA, Algal removal treatment: $R^2 = 0.08$, $F = 0.35$, $p > 0.05$). After algal removal, communities varied significantly between treatments and remained distinct throughout the experiment (PERMANOVA, Algal removal treatment: $R^2 = 0.61$, $F = 31.76$, $p < 0.001$; Month: $R^2 = 0.03$, $F = 0.57$, $p > 0.05$; Treatment x Month: $R^2 = 0.05$, $F = 0.93$, $P > 0.05$; Supplementary Fig. 2a). Algal-removed bommies were dominated by bare substrate (arithmetic mean = 43.8% cover) and turf (28.4% cover), while algal-dominated bommies were dominated by macroalgae (67.8% cover), with the brown macroalgae *Turbinaria ornata* (35.3% cover) & *Dictyota bartayresiana* (13.8% cover) as the two most abundant species (Supplementary Fig. 2b, c). Hard coral cover was low on both algal-removed (6.3% cover) and algal-dominated (2.4% cover) bommies. Six months after algal removal, we sampled the BBL (~50 cm above the substrate) of each bommie, the MBL (~5 cm above the substrate) of the substrate on each algal-removed bommie, and the MBL of substrates dominated by *T. ornata* or *D. bartayresiana* on each algal-dominated bommie (*n* = 12 samples per reef water type; Fig. 1c–e; Supplementary Fig. 3). Measurements by Shashar and colleagues[12] were used to define sampling heights above the substratum for each boundary layer. To explore the origin and diffusion of algal-derived metabolites, we extracted surface- (*n* = 12 samples per species) and endo-metabolomes (*n* = 3 samples per species) from each of the two macroalgal species.
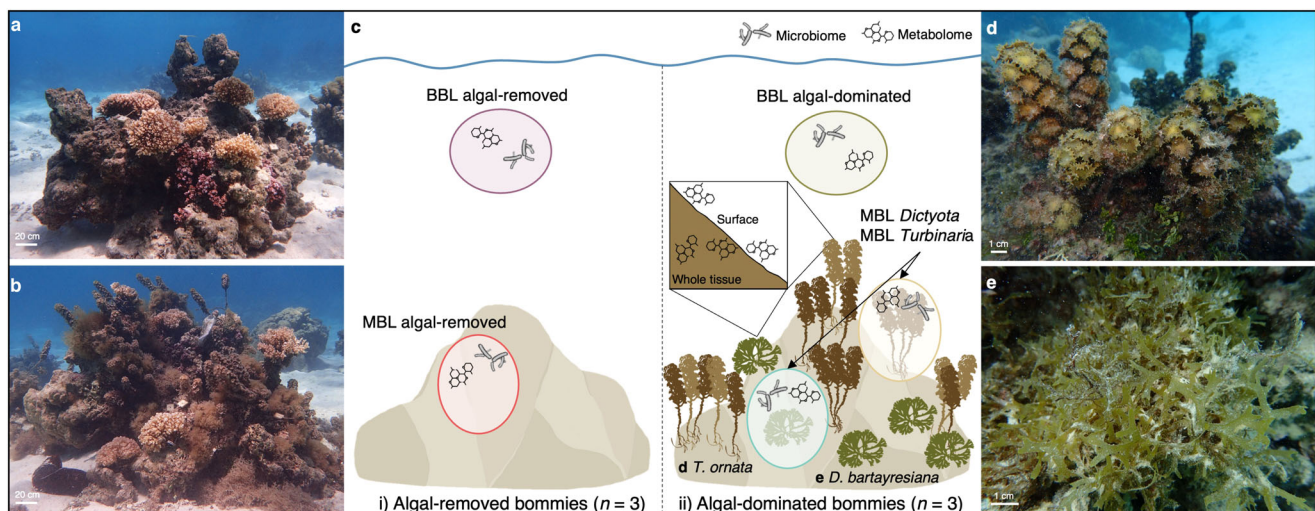

Fig. 1 | Experimental design. Bommies were assigned randomly to two algal treatments: (**a**, **c**) (i) algal-removed and (**b**, **c**) (ii) algal-dominated. Drawings show the location of the different samples: 5 water types represented by the oval shapes on both algal-removed and algal-dominated bommies and, for algal-dominated bommies only, 2 algal surface samples and 2 algal whole tissue samples, i.e., one from each of the two macroalgal species: (**d**) *Turbinaria ornata* and (**e**) *Dictyota bartayresiana*. Both the microbiome and metabolome of water samples were analyzed, while only the metabolome of algal surface and whole tissue samples was considered. BBL Benthic Boundary Layer, MBL Momentum Boundary Layer. *n* = 12 samples per water type. *n* = 12 surface samples per algal species. *n* = 3 whole tissue samples per algal species.
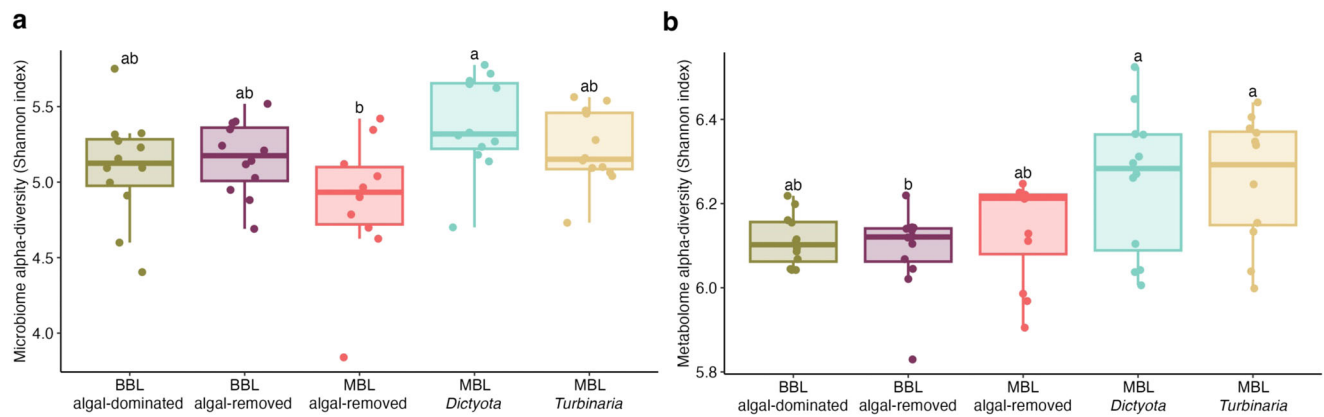
Fig. 2 | Microbial & chemical alpha-diversity across the five reef waters. Shannon diversity index by sample of (**a**) ASVs and (**b**) chemical features. Reef water types are abbreviated and colored as in the experiment design figure (Fig. 1).

Microbial and chemical diversity of reef waters

A total of 5,517 ASVs (Supplementary Data 1) and 975 MS1 features (i.e., dataset 1; Supplementary Data 2) were obtained after data filtration (Supplementary Table 1). Microbiome alpha-diversity (Shannon index) varied significantly between reef water types (ANOVA, $F = 4.01$, $p < 0.01$; Fig. 2a). Specifically, the *Dictyota* MBL showed a higher diversity than the algal-removed MBL (Tukey HSD test, $p < 0.05$). Chemical alpha-diversity varied significantly between reef waters (ANOVA, $F = 4.58$, $p < 0.01$; Fig. 2b), with algal-dominated MBLs being more diverse than the algal-removed BBL (Tukey HSD test, $p < 0.05$).

Compositional differences among reef water microbiomes and metabolomes

We used unconstrained and constrained approaches to explore the microbial (i.e., microbial genera) and chemical (i.e., dataset 2 with MS1 features with MS/MS data; Supplementary Data 3) variations across water types. Unconstrained ordinations (principal component analysis – PCA) of water samples revealed that water types differ in their microbial (PER-MANOVA, $R^2 = 0.13$, $F = 1.99$, $p < 0.001$) and chemical compositions (PERMANOVA, $R^2 = 0.15$, $F = 2.46$, $p < 0.001$; Supplementary Fig. 4; Supplementary Table 2). However, pairwise analysis revealed no significant differences in either microbial or chemical composition between MBL *Dictyota* and MBL *Turbinaria* (pairwise PERMANOVA, $p > 0.05$), nor in chemical composition between BBL algal-removed and BBL algal-dominated samples (pairwise PERMANOVA, $p > 0.05$). We further explored the extent of these compositional differences using partial least squares discriminant analysis (PLS-DA), a supervised method, to evaluate the potential of the microbiome and metabolome to discriminate samples based on their water types. Constrained ordinations confirmed the potential of the microbiome (Supplementary Fig. 5a–d) and metabolome (Supplementary Fig. 5e–h) to differentiate between water types. Notably, the discrepancies between unconstrained and constrained ordinations for the two algal-dominated MBLs and the two BBLs suggest that their compositional differences were subtle, with only key variables distinguishing these water types. We, then, used multi-block PLS-DA analysis, DIABLO[30] to investigate whether the multi-omic signatures of water samples were correlated and could discriminate water types. The first two components of the two ordinations were highly correlated (correlation coefficient > 0.8), showing a strong covariation between both datasets. BBLs significantly clustered apart from each other with only 14% of misclassified samples between algal treatments (Fig. 3a; $CER = 0.14$, $p < 0.01$). Similarly, the multi-omic composition of all three MBLs significantly differed from each other (Fig. 3b; $CER = 0.20$, $p < 0.001$). Additionally, boundary layers were vertically structured regardless of the algal treatment (Fig. 3c, d). The BBL significantly differed from the MBL on both algal-removed (Fig. 3c; $CER = 0.05$, $p < 0.001$) and algal-dominated (Fig. 3d; $CER = 0.19$, $p < 0.001$) bommies.

Dominant microbial taxa across boundary layers and algal treatments

Planktonic microbial communities were dominated by the family Cyano-biaceae (e.g., *Prochlorococcus*), followed by the Actinomarinaceae (e.g., *Candidatus Actinomarina*), Alteromonadaceae (e.g., *Alteromonas*), Flavo-bacteriacae (NS4 and NS5 marine groups), AEGEAN-169 marine group and the SAR86 clades (Supplementary Fig. 6). To identify which genera best discriminated the microbial composition of the five reef water types, we summed the VIP scores of the 409 discriminant genera across the former four PLS-DA models (Supplementary Fig. 5a–d) and focused on the 50 ASVs with the highest summed scores (Fig. 4). Genera belonging to the Gammaproteobacteria and Bacteriodia were particularly abundant in algal waters. Specifically, the algal-dominated BBL and MBLs were enriched in the Gammaproteobacteria *Legionella*, two Bacteroidia *Leeuwenhoekiella* (family Flavobacteriaceae) and *Owenweeksia* (Cryomorphaceae), and some Alphaproteobacteria, such as *Epibacterium* (Rhodobacteraceae). Both algal-dominated MBLs also harbored a high abundance of the Gammaproteo-bacteria *Alcanivorax, Halomonas, Idiomarina, and Marinobacter*. Numerous Alphaproteobacteria were enriched in these MBLs including *Croceicoccus* (Sphingomonadaceae), *Henriciella, Maricaulis* (Hyphomo-nadaceae), and *Pelagibaca* (Rhodobacteraceae). A few ASVs differentiated the two algal-dominated MBLs. For the *Dictyota* MBL, these included the Gammaproteobacteria *Oceanococcus* and *Candidatus Uhrbacteria* (ABY1) and, for the *Turbinaria* MBL, several Alphaproteobacteria (e.g., *Aestuar-iicoccus, Nautella* and *Sagitulla* from the Rhodobacteraceae) and the Gammaproteobacteria *XY-R5* (Alteromonadaceae). In contrast, algal-removed waters were characterized by an enrichment of Alphaproteo-bacteria, including *Nitratireductor* and *Oricola* (Rhizobiaceae) in the BBL, and *Aestuariicoccus, Mameliella, Roseitalea,* and *Sagittula* in the MBL.

Diffusion pattern of macroalgal metabolites across boundary layers

To explore the diffusion of algal-derived metabolites into the algal boundary layers, we processed algal whole tissue, algal surface, and algal-dominated water samples together to built a quantitative table comprising 3943 MS1 features after data filtration (Supplementary Data 3). PLS-DA indicated that metabolomic signatures strongly discriminated sample types for both algal species (Fig. 5a; *Dictyota*: $CER = 0.11$, $p < 0.001$; *Turbinaria*: $CER = 0.13$, $p < 0.001$). Chemical compositional differences between sample types were confirmed by unconstrained PCA and PERMANOVA (Supplementary Fig. 7; Supplementary Table 3). On the 1st component, metabolite features from algal surfaces and whole tissues clearly clustered apart from the water samples, while the 2nd component separated the algal surface and water samples from the whole tissue samples. Interestingly, the level of differentiation was lower between adjacent sample types (e.g., Surface vs. MBL) compared to distant ones (e.g., Tissue vs. BBL; pairwise PERMANOVA;
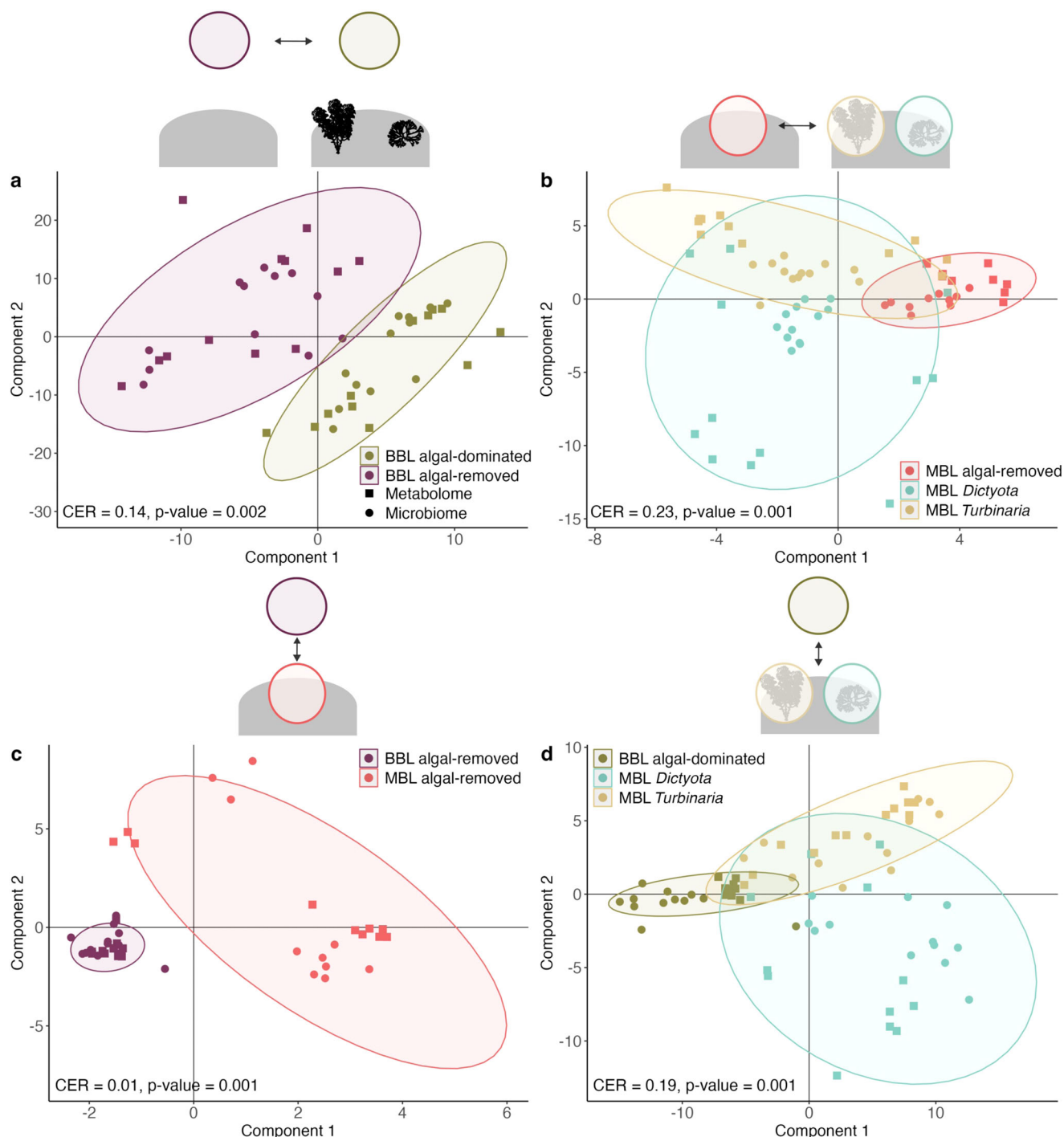
Fig. 3 | Multi-omic composition of reef boundary layers. Score plots of the multiblock PLS-DA (DIABLO) performed on metabarcoding and metabolomic data between (**a**) benthic boundary layers (BBL), (**b**) momentum boundary layers (MBL), (**c**) algal-removed waters, and (**d**) algal-dominated waters. Analyses were validated by a permutation test based on cross-model validation. The CER (classification error rate) represents the proportion of misclassification and a $p < 0.05$ indicates that the clustering was not obtained by chance alone. Ellipses represent the spread of data points at a 95% confidence level. Reef water types are abbreviated and colored as in the experimental design figure (Fig. 1). Individual PLS-DAs are shown in Supplementary Fig. 5.

Supplementary Table 3). The distinct chemical signatures of whole tissue and surface were confirmed by a substantial number of metabolites specifically detected in each sample type (Fig. 5b). Interestingly, a high proportion (~30%) of metabolites were shared across all sample types for both algal species. We hypothesized that algal compounds would diffuse across boundary layers according to their polarity, with hydrophobic compounds more likely to be retained close to producing organisms and polar compounds more likely to move across boundary layers. By using

chromatographic retention time as a proxy for polarity (i.e., in reverse phase column, polar compounds tend to be eluted first), we found a stepwise decrease in retention time, with each feature weighted equally, from the algal whole tissue to the algal-dominated BBL, supporting our hypothesis (Fig. 5c; Kruskal-Wallis, *chi-squared* = 1200.4, $p < 0.001$). Interestingly, a similar pattern was observed in abundance-weighted retention times (Supplementary Fig. 8)., suggesting that polarity influenced both the diversity and relative abundance of features across sample types

Fig. 4 | Reef waters-associated discriminant microbial taxa. Benthic boundary layers (BBL) were collected above algal-dominated and algal-removed bommies. Momentum boundary layers (MBL) were associated to algal-removed substrate or above macro-algal species: Dictyota bartayresiana and Turbinaria ornata. Microbial amplicon sequence variants (ASVs) are at the genus-level and labeled at the family and genus level. ASVs are colored according to their microbial class and clustered according their mean CLR transformed abundances across the five water types using Euclidian distances and Ward's minimum variance method. Data was scaled by mean-centering and dividing by the standard deviation.
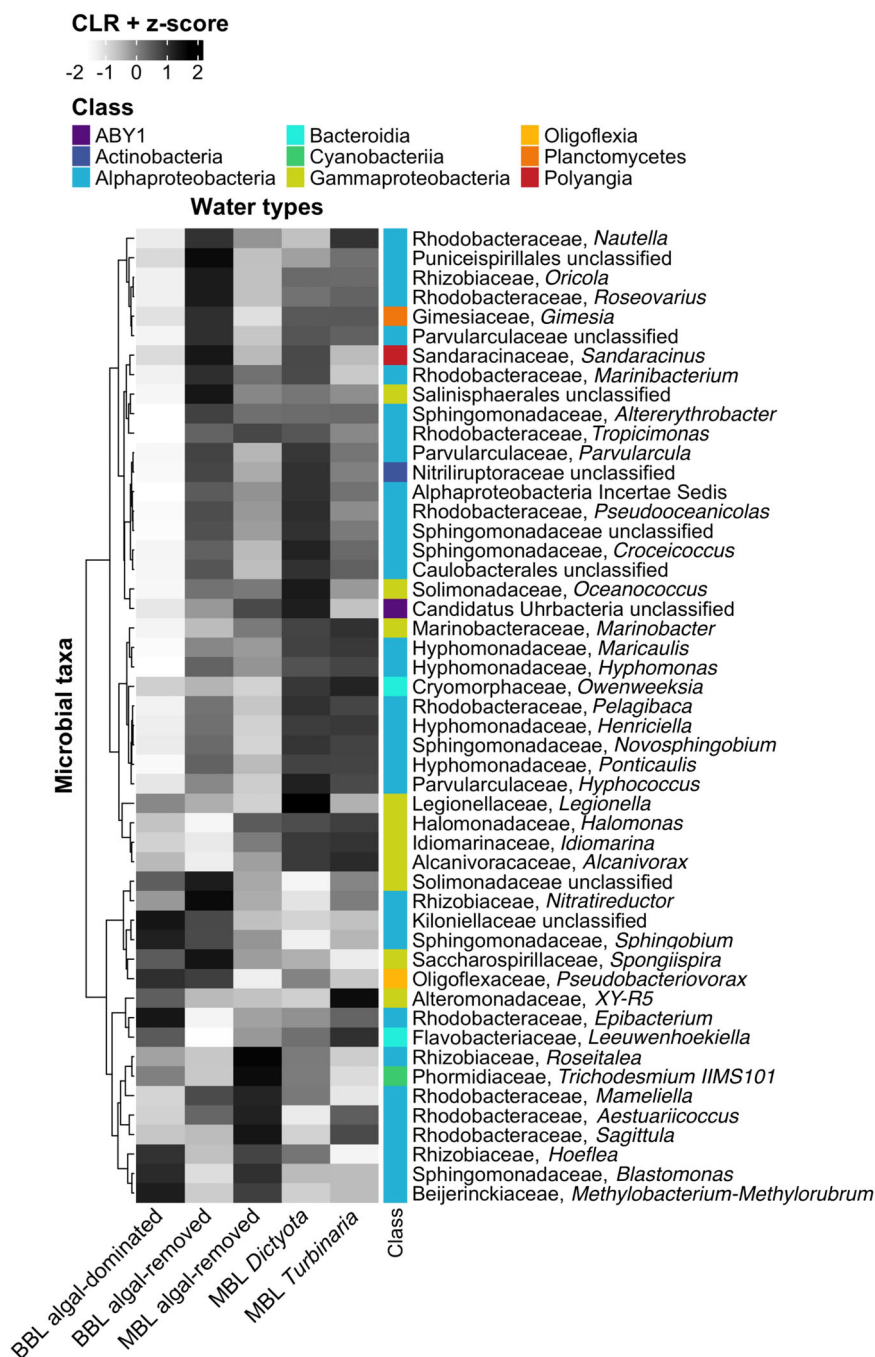
Broad molecular classification of diffusing algal-derived metabolites

To further investigate the chemical diversity of diffusing algal-derived metabolites, we retrieved the consensus MS2 spectra of each ion feature obtained from the concurrent processing of algal tissue, surface and water spectral data for molecular networking (see "*Methods*"). The Feature-Based Molecular Network analysis on GNPS[24,31] grouped the 4585 initial MS1 features with consensus MS2 fragmentation spectra into 436 subnetworks based on their spectral similarity (i.e., molecular networks of alike features; Fig. 6a), of which 2214 clustered into 256 subnetworks after filtration (i.e., dataset 2; Supplementary Data 3; Supplementary Data 4). To highlight relevant subnetworks of diffusing algal-derived metabolites, we hypothesized that molecules are produced in algal whole tissue and/or surface and gradually diffuse in the upper water layers (i.e., presence in the MBL and, possibly, the BBL). Therefore, we selected, for each algal species,

subnetworks that had at least 3 discriminant features (VIP score > 1), or at least 1 feature with a VIP score superior to the median that were at least detected in either or both whole tissue or surface and in the MBL. A total of 316 features comprised the 58 subnetworks obtained, of which 20 and 13 were exclusively associated with *Dictyota* and *Turbinaria*, respectively (Fig. 6a; Supplementary Table 4; Supplementary Data 4). Finally, each subnetwork was broadly annotated using the ClassyFire ontology[32] via MolNetEnhancer on GNPS[23], CANOPUS on SIRIUS[25,33], and manual verifications of spectral matches and library search.

Subnetwork classification illustrated patterns of differential diffusivities according to chemical classes among the four sample types for both algal species (Fig. 6c). In general, subnetworks affiliated to prenol lipids, fatty acyls, and glycerolipids showed a diffusion-like profile with decreasing mean relative abundances from algal whole tissue to algal-dominated BBL (Supplementary Fig. 9a–c; Supplementary Table 4).
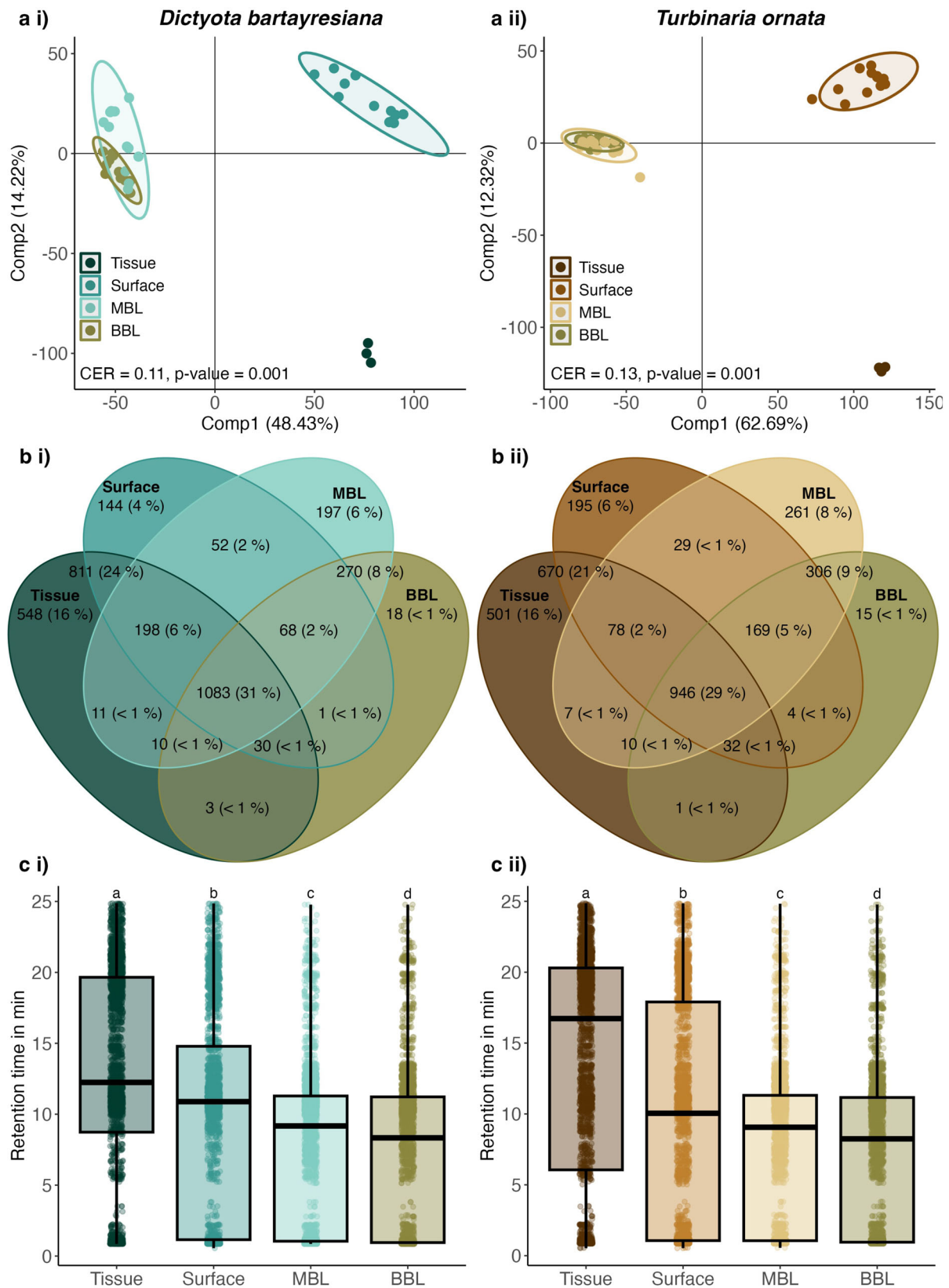
Fig. 5 | Analysis of algal metabolites diffusion into the water column for (i) *Dictyota bartayresiana* **and (ii)** *Turbinaria ornata*. **a** PLS-DA score plots of MS1 features with MS/MS fragmentation spectra (*n* = 2214 features) showing metabolomic profiles clustered according to algal whole tissues, surfaces, MBLs, and BBL. Metabolites relative peak areas were CLR-transformed and mean-centered. CER and associated *p* values were obtained by cross-model validation and permutation tests. Ellipses represent the spread of data points at a 95% confidence level. (**b**) Venn diagrams of MS1 features in whole tissues, surfaces and MBLs of *Dictyota* (*n* = 3444) and *Turbinaria* (*n* = 3224) and algal-dominated BBL (*n* = 1661). **c** Unweighted retention time of each feature in minutes using UHPLC reverse phase column. Lettering indicates significant differences using Dunn test's posthoc *p* < 0.05. BBL Benthic Boundary Layer, MBL Momentum Boundary Layer.
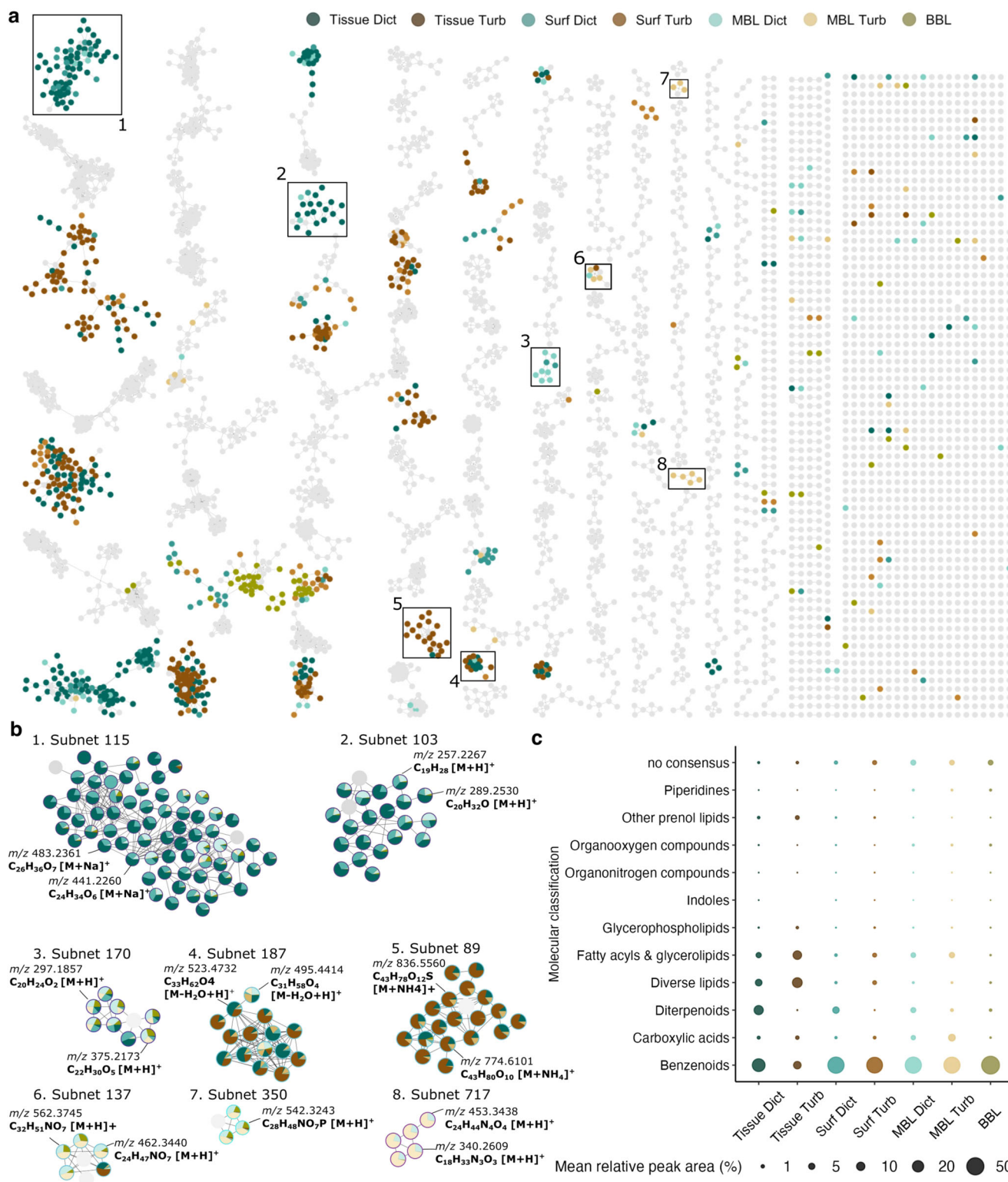
Fig. 6 | Molecular classification of subnetworks with discriminant features found in the algal metabolomes and associated waters. a Molecular network of all MS1 features (nodes) with MS/MS fragmentation spectra linked by a cosine score >0.7 (edges). Nodes are colored by the sample type in which their relative abundance was the highest. Examples of subnetworks of interest with discriminant features found in whole tissue & surface samples and boundary layers (BBL—benthic & MBL— momentum) of the two algal species *Dictyota bartayresiana* and *Turbinaria ornata* are boxed 1–8. **b** Boxed subnetworks details in which nodes are colored by their mean relative intensities (i.e., peak areas) in each sample type. **c** Mean of summed features relative intensities of subnetworks of interest across sample types according to their consensus ClassyFire chemical ontology derived from MolNetEnhancer (GNPS) and CANOPUS (SIRIUS) outputs.

Diterpenoids were the most prominent metabolites in *Dictyota*-associated samples (Fig. 6a–c; Supplementary Fig. 9a) and, collectively, they summed to 16.7%, 7.5%, 4.3% of the total peak areas in *Dictyota* whole tissue, surface and MBL, respectively. They were rare in *Turbinaria* whole tissue and surface (<0.02% of the total peak areas), but present in *Turbinaria* MBL (1%). Several diterpenoids may be related to spatane and secospatane derivatives, including subnetwork 115 (Fig. 6b1; Supplementary Table 5a), subnetwork 103 (Fig. 6b2; Supplementary Table 5a) and subnetwork 170 (Fig. 6b3; Supplementary Table 5a). Despite not being flagged as discriminant features, we detected two features with masses and putative formulas very closely matching known allelopathic diterpenoids isolated from *Dictyota*[34,35], including Crenulacetal C ($C_{24}H_{38}O_5$, subnetwork 115; Fig. 6b1) and Pachydictyol A ($C_{20}H_{32}O$, subnetwork 103, Fig. 6b2; Supplementary Table 5a). However, we cannot rule out that these features are isomers with different chemical and biological properties. Sesquiterpenoids constituted another subclass of prenol lipids characteristic of *Dictyota* whole tissue and surface (subnetwork 493; Supplementary Fig. 9b; Supplementary Table 4). For *Turbinaria*, discriminant prenol lipids were rather related to carotenoids (e.g., subnetwork 214; Supplementary Table 5a), summing to 0.3% of the total peak areas. The relative abundances of fatty acyls and glycerolipids in whole tissue and surface samples were three-fold higher in *Turbinaria* compared to *Dictyota*, summing up to 4.6% and 1.5% of the total peak areas, respectively (Fig. 6c; Supplementary Fig. 9c; Supplementary Table 4). Some noteworthy examples are subnetwork 187 composed of monoacylglycerols and diacylglycerols (e.g., DAG (16:0/14:0); Fig. 6b; Supplementary Table 5a) and subnetwork 89 composed of monogalactosyl diacylglycerol (e.g., MGDG (18:1/16:0); Fig. 6b5; Supplementary Table 5a). In addition, two features from subnetwork 89 were annotated as sulfoquinovosyl diacylglycerol (e.g., SQDG (34:2); Supplementary Table 5a). Discriminant features of glycerophospholipids were detected in four subnetworks and were less prominent in algal whole tissue and surface than the previously discussed lipid classes, making up to 0.1% and 0.04% of total peak areas for *Turbinaria* and *Dictyota*, respectively (Fig. 6c; Supplementary Fig. 9d; Supplementary Table 2). Algal-dominated MBLs and BBLs were characterized by an enrichment of some subnetworks of these lipid classes compared to whole tissue and surface samples (Supplementary Fig. 9c, d; Supplementary Table 4). They were constituted of lipids in their lyso forms, such as subnetwork 137 associated to lyso-betaine lipids (e.g., Lyso DGCC (22:6); Fig. 6b6; Supplementary Table 3a) and subnetwork 350 associated to lyso-phosphatidylcholines (e.g., Lyso-PC (20:5); Supplementary Table 5a). In addition, features annotated as benzene derivatives (e.g., subnetwork 13) were prominent in algal-dominated MBLs and BBL comprising about half of the total peak area (Fig. 6c; Supplementary Fig. 9e; Supplementary Table 4). Other molecular classes characteristic of algal-dominated MBLs and BBL included organooxygen compounds (e.g., subnetwork 33), organonitrogen compounds, carboxylic acids (e.g., subnetwork 717; Fig. 6b8; Supplementary Table 5a), piperidines and indoles (Fig. 6c; Supplementary Fig. 9f–j; Supplementary Table 4).

Finally, we investigated the subnetworks in negative ionization mode. The dataset was less than half the size of the dataset in positive mode with 1,029 features and 83 subnetworks after filtration (Supplementary Data 5). Fewer molecular classes could be resolved across the 24 selected subnetworks, and only 13 subnetworks were annotated (Supplementary Fig. 10; Supplementary Data 6). An additional molecular class was identified, the organic sulfuric acids, which were abundant in algal surfaces and waters. Features identified as organooxygen compounds were the most prominent across all samples in adequation with their better ionization and fragmentation in negative mode. Summed together, they comprised 51.4% and 46.6% of the total peak areas for *Dictyota* and *Turbinaria*, respectively. Sugar alcohols (subnetworks 55 and 126; e.g., Mannitol library match; Supplementary Table 5a) were particularly abundant in algal whole tissue and surface, while carbohydrates (subnetwork 2) were rather abundant in algal-dominated MBLs and BBL (Supplementary Fig. 10b).

Co-variation of algal-associated metabolites and microorganisms

To investigate the associations between previously identified discriminant metabolites ($n = 316$ features) and microorganisms ($n = 207$ microbial genera), we integrated the metabolomic and metabarcoding data from both algal MBLs using the multi-block PLS-DA analysis DIABLO[30]. We excluded the algal-dominated BBL to address species-specific differences within the same boundary layer and avoid confounding factors. DIABLO revealed a strong association between the metabolome and microbiome of the algal MBLs with a distinct cluster for each algal species (correlation coefficient > 0.95; Supplementary Fig. 11). The analysis selected 26 metabolites and 27 ASVs with a strong correlation coefficient (<−0.7 or >0.7) and resulted in a bipartite network comprising three clusters (Fig. 7). In the first cluster (Fig. 7a), two diterpenoids (Supplementary Table 5b), an organonitrogen compound, an organooxygen compound, a piperidine ($C_{14}H_{18}N_2O_2$), a carboxylic acid and the Lyso-PC (20:5) were negatively correlated with diverse ASVs belonging to *Alistipes, Eilatimonas, Rikenella,* and *Roseibacterium*, and two unclassified taxa from the Desulfovibrionaceae and Victivallaceae families. These ASVs were also involved in positive relationships with a cyclopeptide ($C_{18}H_{33}N_3O_3$, subnetwork 717), possibly related to a halolitoralin and a glycerophospholipid. An unknown third diterpenoid was negatively correlated to *Ketobacter, Mycobacterium* and *Pseudooceanicola* which were also positively correlated to the organonitrogen and organooxygen compounds and the carboxylic acid. These compounds interacted also positively with the genera *Acanthopleuribacter* and *Hyphomonas*. *Tropicibacter* was negatively correlated to an organooxygen compound and an unknown metabolite connecting a second part of the cluster comprising *Ponticaulis, Roseovarius* and a Patescibacteria (JGI 0000069-P22). The second cluster (Fig. 7b) comprised lipids, such as the SQDG (14:0/18:4) and the MGDG (16:3/20:5), and an amino acid ($C_6H_{16}N_4O_2$), which interacted negatively with *Citreicella* and *Oleibacter*. The third cluster (Fig. 7c) included only negative correlations between diterpenoids and *XY-R5*. Two of these diterpenoids belonged to the subnetwork 115 ($C_{24}H_{34}O_6$ and $C_{26}H_{36}O_7$; Fig. 6b1; Supplementary Table 5a, b). These metabolites were detected in higher abundances in the *Dictyota* MBL, while *XY-R5* was relatively more abundant in *Turbinaria* MBL. In contrast, *Calorithrix* was positively correlated with two of these metabolites and was enriched in *Dictyota* MBL.

In addition, we investigated associations between microbes and the discriminant metabolites ($n = 216$ features) from the dataset in negative ionization mode (Supplementary Fig. 12; Supplementary Table 5c). Briefly, two organic sulfuric acids and a diterpenoid were negatively correlated to *Alistipes* and *Eilatimonas*, which interacted positively with a phenol and an organooxygen compound. In contrast, this phenol was negatively correlated with *Ketobacter* and *Mycobacterium* (Supplementary Fig. 12a). Sulfolipids were negatively correlated with *XY-R5* and positively correlated with *Calothrix, Pseudoruegeria* and *Roseibacterium*, (Supplementary Fig. 12b). Finally, this analysis revealed positive associations between various carbohydrates (e.g., pentose, aminoglycoside), a carboxylic acid, and several ASVs belonging to *Oleibacter, Ponticaulis* and *Tropicibacter* (Supplementary Fig. 12c).

Discussion

On coral reefs, the tight coupling between microorganisms and metabolites drives reef biogeochemical processes and mediates ecological interactions[1,3]. In the wake of the widespread shift from coral to macroalgal dominance, deciphering the unseen diversity of microbes and chemicals and their spatial distribution is paramount to understand the consequences of benthic community changes on coral reef ecosystem function and resilience. Here, we demonstrate that macroalgal assemblages modify chemical and microbial waterscapes surrounding coral bommies. Our analyses identified specific classes of algal-derived
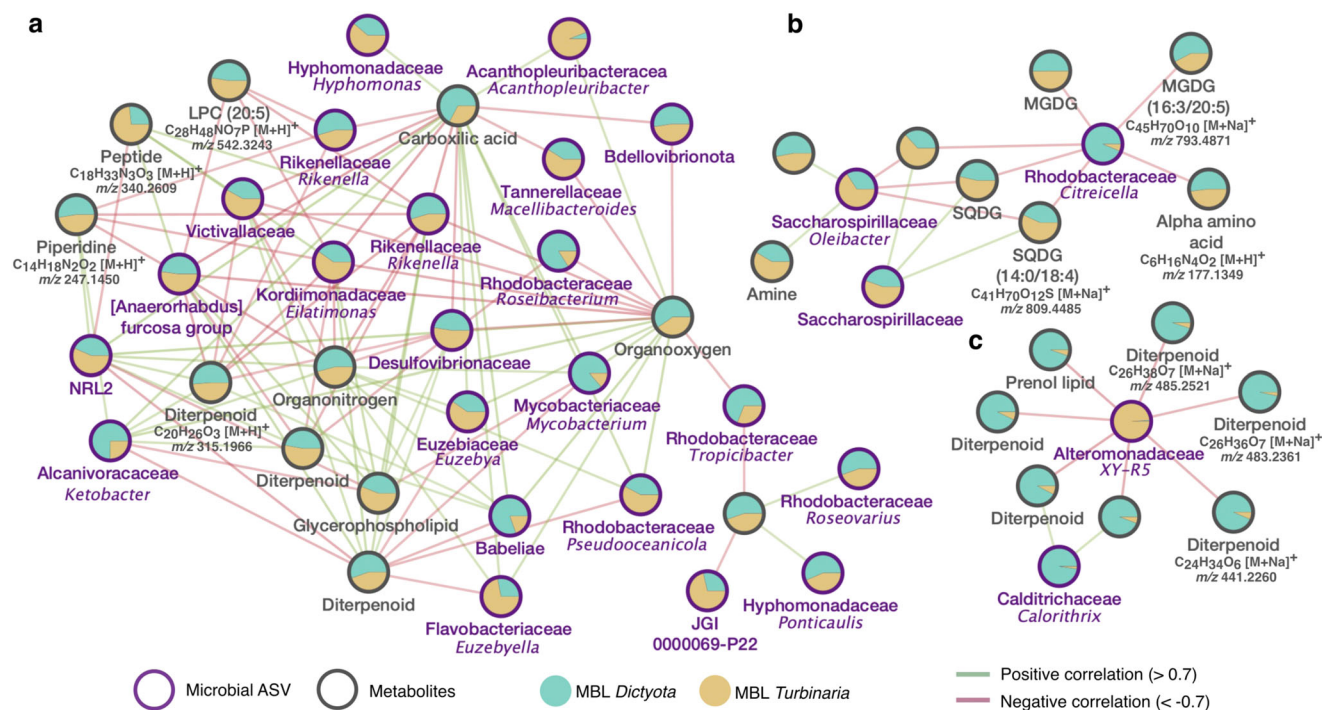
Fig. 7 | Co-variation of discriminant microbial amplicon sequence variants (ASVs) and molecular features in algal momentum boundary layers (MBLs). Bipartite correlation network obtained from DIABLO analysis and visualized on Cytoscape. A correlation threshold was set to 0.7 resulting in three clusters (**a**, **b**, **c**). Nodes are contoured according to their type (i.e., ASVs in purple and metabolites in gray) and colored by their mean relative intensities (i.e., peak areas) in the MBL of *Dictyota bartayresiana* and *Turbinaria ornata*. Putative annotations are shown in Supplementary Table 5a, b.

metabolites, including diverse lipids classes (e.g., prenol lipids and gly-cerolipids) and labile organic matter (e.g., organooxygen compounds and carboxylic acids). Several of these classes featured a diffusion profile with decreasing relative abundance from the whole tissue to the BBL, which is consistent with the hypothesis that hydrophobic compounds remain close to emitters, while polar compounds move across boundary layers. In addition, microbiome-metabolome data integration highlighted strong co-variations between algal-associated metabolites and microbes, overall suggesting that some of these metabolites could structure microbial communities in coral reef waters.

Our study shows a remarkable spatial heterogeneity in microbial and chemical waterscapes according to dominant benthic taxa and boundary layers under real flow condition. Horizontally, the description of distinct pools of bacteria and metabolites in each boundary layer between algal-dominated and algal-removed bommies is congruent with previous studies at the organismal[10,18] and reef[14,16,17] scales. Consistent with earlier research on microbial communities[10,18], we also observed a vertical separation between the MBL and BBL surrounding both algal-dominated and algal-removed bommies. This spatial structuring is likely driven by interacting biological and physical processes. The hydrodynamic conditions, such as flow velocity and turbulences, within each boundary layer regulate the advection of benthic organic matter and microorganisms[12,13]. In addition, the rates at which metabolites and microbes are released into the water column, along with their interactions, further determine the occurrence of chemical and microbial concentration gradients[27,36]. However, some studies did not detect differences between surface and benthic waters in microbial assemblages[37] and chemistry[9]. Interestingly, the multi-omic signatures of BBLs surrounding algal-dominated and algal-removed bommies were clearly distinct. Although reef currents are expected to homogenize upper water layers, the presence of canopy-forming macroalgae, such as *Turbinaria* and *Sargassum*, likely reduces flow velocity and increases turbulence, which, in turn, may increase the retention of molecules and microbes within the BBL[38].

By exploring metabolite pools from the algal tissue to the algal-dominated BBL, this work provides a fine-scale spatial characterization of algal-derived metabolites within the reef ecosystem. For both algal species, the surface metabolome lied between the endo-metabolome and the two boundary layers (i.e., the MBL and BBL), highlighting holobiont surfaces as key interaction zones between the host, its epibiont community and its surrounding environment[7,27]. In addition, a substantial proportion of surface- and endo-metabolites were detected across the boundary layers, supporting the existence of chemical gradients in the water column[27]. By relating the diversity and relative abundance of metabolites to their chromatographic retention times from the algal tissue to the algal-dominated BBL (Fig. 5c), our results suggest that algal-derived metabolites diffuse into the water column according to their polarity. This finding supports that hydrophobic compounds will act on contact or diffuse at a very short distance, while medium polar or hydrophilic compounds will have a wider range of detection and potential activities.

Using spectral library matches and in silico annotations, our study demonstrates that the diffusivity of metabolites across boundary layers differs according to their molecular classes. In a recent study, metabolites from diverse lipid classes, including prenol lipids, fatty acyls, glycerolipids, and glycerophospholipids, were abundantly recovered from tropical green and red macroalgae which is congruent with our results[22]. We found that metabolites associated to sesquiterpenoids, carotenoids, and sulfolipids were abundant in the algal tissue and surface but scarce in algal waters. This limited diffusion is consistent with their surface-bound anti-fouling and cytotoxic properties[39–41]. In contrast, diterpenoids, conspicuous in *Dictyota* tissue, were also abundant in the *Dictyota* MBL and the algal-dominated BBL (Fig. 6c). While diterpenoids display a range of contact-dependent bioactivities, ranging from herbivore deterrence to allelopathy[42–44], this finding indicates a water-borne action and/or a high release rate by macroalgae. In contrast, benzenoids, organooxygen compounds, carboxylic acids, and lysolipids were abundantly detected in the algal MBLs and algal-dominated BBL (Fig. 6c; Supplementary Fig. 9). Their high abundance in the boundary layers suggests a non-specific origin of these compounds. For

Fig. 8 | Conceptual diagram of chemical and microbial waterscapes above the algal-dominated bommies. Algal-derived metabolites vary in their diffusivities across boundary layers (i.e., BBL and MBL), with some metabolites displaying diffusion-like profile (e.g., diterpenoids, glycerolipids). The emergence of chemical gradients structure microbial assemblages according to the molecular classes and the ecological roles of these metabolites. Metabolites can constitute trophic resources (e.g., organooxygen compounds) or allelopathic agents (e.g., diterpenoids, sulfolipids). Within the algal waterscapes, two mechanisms could contribute to coral demise and reinforce phase-shifts: water-mediated allelopathy and the virulence of copiotroph microbes fed by algal-derived OM. Allelochemicals (e.g., diterpenoids) and potential virulent bacteria (e.g., Alcanivorax) could negatively impact coral health during the pelagic larval and sedentary benthic phases, which urgently require further experimental investigations. BBL Benthic Boundary Layer. MBL Momentum Boundary Layer.
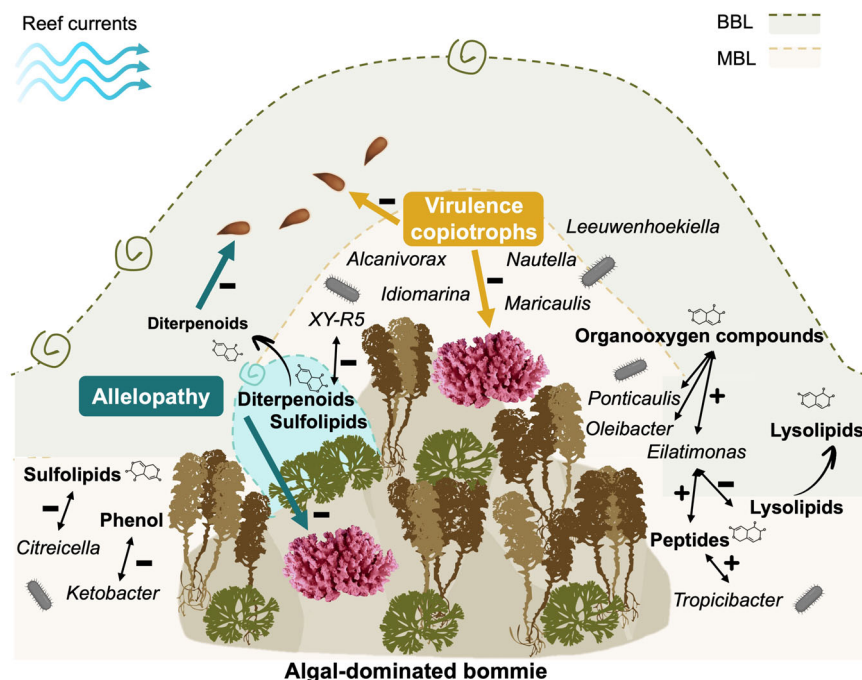
instance, benzenoids are released by diverse organisms, such as phytoplankton[45], turf, and corals[21]. Organooxygen compounds also constitute important growth and energy substrates for microbial life[4,46]. While variations in physiochemical properties (e.g., size, polarity[36]) might account for the different abundance profiles observed among the sub-categories of organooxygen compounds (Supplementary Figs. 9 and 10), these differences might also imply distinct lability and, therefore, biotransformation rate by microbes. Finally, the structural property of lysolipids, consisting of a single fatty acyl chain and a polar head, might make them more hydrophilic than other lipids[47]. While we highlight polarity as a potential factor influencing metabolite diffusion, future investigations into the other aforementioned factors will be paramount to understand the determinants and extent of these chemical gradients in reef waters.

Our integrative approach reveals a strong co-variation between microbiome and metabolome datasets, supporting a tight microbe-metabolite coupling in the coral reef waterscape. The observed enrichment of Gammaproteobacteria and Bacteroidia in algal waters echoes numerous studies demonstrating the selective influence of energy- and carbon-rich algal exudates on these microbial classes[1,4,20]. The algal MBLs and algal-dominated BBL harbored several genera from these classes known for their copiotrophic lifestyle and capacity to degrade complex OM, including *Alcanivorax, Eilatimonas, Idiomarina, Leeuwenhoekiella* and *Oleibacter*[46,48–50]. In addition, the Alphaproteobacteria *Croceicoccus* and *Hoeflea*, abundant in the algal waters, can metabolize mannitol as their carbon source[51,52]. In fact, organooxygen compounds constituted a significant proportion of the algal MBLs, particularly in negative ionization mode (Fig. 6c; Supplementary Figs. 9 and 10). Besides carbohydrates, carboxylic acids can also constitute strong chemo-attractants and foraging cues for coral reef bacteria[53,54], including from the Rhodobacteraceae, which is consistent with the observed positive correlations in microbe-metabolite network (Fig. 7; Supplementary Fig. 12). Although the analysis of data in positive ionization mode prevails in coral and reef metabolomics and yields a greater number of putative annotations, our results encourage the exploration of negative ionization metabolomics to gain a better understanding of microbe-metabolite interactions.

The enrichment of copiotrophic lineages has often been described as indicative of high macroalgal cover and signs of reef microbialization[1,14,17]. In addition, these copiotrophs can constitute virulent microbial populations

capable of shifting towards a pathogenetic lifestyle when labile carbon is abundant[4,14,46]. For example, *Alcanivorax*, enriched in the algal MBLs (Fig. 4), has previously shown such metabolic versatility[46]. Copiotrophic microbes can invade stressed and diseased corals[55,56], and several taxa characteristic of the algal MBLs are suspected to be coral[57,58] and algal[59,60] pathogens, among them *Halomonas, Maricaulis* and *Nautella* (Fig. 4). However, some taxa (e.g., *Halomonas*) can also be beneficial bacteria[61], calling for cautious interpretation of their putative roles beyond their taxonomic affiliations. Comparatively, *Roseitalea* and *Mameliella*, two probiotic bacteria of corals and Symbiodiniaceae[62,63], were depleted in algal waters. Allelopathy could also represent a threat to coral holobionts. In particular, several studies on hard corals and sponges demonstrated the cytotoxicity of diterpenoids and SQDGs[41,42]. In this context, we propose a conceptual model for the spatial structuring of chemicals and microbes around algal-dominated bommies (Fig. 8). In this model, algal-derived metabolites act as structuring elements of planktonic microbial communities. We posit that boundary layers surrounding algal-dominated bommies harbor metabolites that could foster reef degradation through allelopathy and the virulence of copiotrophs. However, the extent to which these water-borne elements are effectively detrimental to underlying benthic corals, as well as their pelagic stages, urgently requires further investigation. This model is consistent with the DDAM (Disease, Dissolved organic carbon, Algae, and Microbe) and reef microbialization hypothesis, which supports a link between elevated DOC concentrations and the emergence of potential coral pathogens[14,28,46].

The algal MBLs harbored DMSP-degrading bacteria (e.g., *Idiomarina and Marinobacter*)[64]. DMSP is a significant substrate and chemical mediator for bacterioplankton[65]. It is produced by coral- and algal-associated bacteria[64], as well as free-living taxa, including *Pelagibaca* and *Pseudooceanicolla*[66], two Rhodobacteraceae which were enriched in the algal MBLs. Nitrogen transformation on coral reefs is complex and largely mediated by microbial activity[2]. Some of the detected taxa, such as *Acuticoccus* and *Nitratireductor*, may be involved in these processes[67]. Strong microbial interactions with sulfur- and nitrogen-containing compounds were revealed in our analysis of bipartite networks (Fig. 7; Supplementary Fig. 12), further supporting their structuring role in planktonic assemblages. Conversely, negative microbe-metabolite associations occurred with diterpenoids, SQDGs, phenols, and Lyso-PC (Fig. 7; Supplementary Fig. 12),

which can inhibit bacterial settlement and growth[35,68,69]. Surprisingly, diterpenoids were also abundant in *Turbinaria* MBL, likely due to the presence of epiphytic *Dictyota* on *Turbinaria* thalli, thereby suggesting a chemically-mediated associational benefit between both algae[70]. In tropical macroalgae, lysophosphatidylcholines may be determinant in the establishment of host-microbe symbiosis, mediated by host immunity pathways[22]. Positive associations between these lipids and microbes from the Saprospiraceae, Flavobacteriaceae, and Rhodobacteraceae families have been reported in algal tissues[22], while our observations revealed negative associations with two genera from the Rikenellaceae family in algal waters. Additionally, metabolites may be of bacterial origin, such as the cyclopeptide (Fig. 7a; Supplementary Table 5a) related to halolitoralin, an antifungal cyclopeptide produced by marine bacteria[71]. Although our study focused on algal waters, it contributes to deciphering the microbe-metabolite pairings associated with macroalgal holobionts. Promising future research should investigate the consistency of these patterns across algal tissues, surfaces, and the surrounding environment to further our understanding of ecological interactions within coral reef systems.

Despite a broad classification system, our work demonstrates that coral reef macroalgae release a variety of compounds potentially involved in defensive and competitive interactions, as well as in microbial energetics[21,35,42]. However, minor modifications in the structure of compounds can change their bioactivity, making the prediction of their effects solely based on their class identities ambitious[72]. We also cannot rule out that the mentioned microbe-metabolite co-variations are not causal. Moreover, it is important to note that the relative abundance of metabolites does not necessarily reflect their absolute amounts. Quantification using appropriate standards is essential to confirm the actual concentrations of these metabolites in the samples. Without an accurate quantification of metabolite concentrations, a better annotation of unknown metabolites, and improved knowledge of the ecology of reef microbes, determining the nature of microbe-metabolite interactions will remain highly challenging. Future research should isolate specific metabolites and conduct bioassays to elucidate their role in microbial processes and interspecific interactions. Importantly, only a fraction of the chemical pool can be successfully retrieved as the successive steps of extraction, ionization, fragmentation, and annotation narrow down the pool of studied compounds, leaving a vast unknown "dark" fraction[26]. While the recent advent of in silico tools have revolutionized compound dereplication, achieving confident annotations, even at a broad level, remains highly challenging, especially for the marine environment with limited spectral libraries[26]. Overcoming these limitations will be crucial for advancing marine metabolomics and multi-omics.

This study provides key insights into the influence of macroalgal assemblages on chemical and microbial waterscapes. The taxonomic composition of the microbial communities revealed an enrichment of copiotrophic bacteria, characteristic of altered reef states and compromised coral holobionts, in two boundary layers overlying macroalgal-dominated bommies. By characterizing the broad molecular classification of algal-derived metabolites, this work participates in the description of the chemodiversity on coral reefs and improves our understanding of water-mediated transport of chemical compounds and their roles as structuring and functioning elements. The data presented herein contribute to further unveil the identity, distribution and co-variations of metabolites and microbes within reef waterscapes and constitute a starting point to further investigate their complex roles in coral reef functioning and resilience. It also provides leads for more targeted research to explore the water-mediated mechanisms by which coral reef macroalgae reinforce the persistence of coral-algal phase-shifts.

Methods
Study site and experimental design
This study took place in a shallow fringing reef lagoon (2–2.5 m deep) of Mo'orea, French Polynesia (17°29'14.86"S 149°53'0.76"O) between June 2020 and June 2021. In late June 2020, six coral bommies (1–2 m diameter) densely covered by macroalgal assemblages were randomly selected within an area of ~1000 m² (Supplementary Fig. 1). Bommies were randomly assigned to one of the two treatments: (i) algal-dominated (i.e., macroalgae left untouched) and (ii) algal-removed (i.e., macroalgae removed including canopy-forming holdfasts and understory species). Macroalgae were removed from their substratum manually and with wire brushes, taking care not to damage other benthic organisms or to alter the substrate microtopography. Their absence on algal-removed bommies was maintained on a monthly basis. Benthic communities were monitored by photographing 5 randomly placed 20 × 20 cm quadrats on each bommie. A first monitoring was conducted before algal removal in June 2020. Subsequent monitoring was performed in August 2020, November 2020, February 2021, and May 2021. Benthic categories included: bare substrate (i.e., absence of macroorganisms but presumably colonized by microalgae), crustose coralline algae (CCA), cyanobacteria, living hard coral, algal turf (i.e., mixed species assemblages of filamentous algae <1 cm in height) and macroalgae (upright and anatomically complex algae with canopy height >1 cm). Within the macroalgae category, 8 genera or species were recorded: *Amansia rhodantha, Chnoospora* spp., *Dictyota bartayresiana, Halimeda* spp., *Lobophora* spp., *Padina boryana, Sargassum pacificum* and *Turbinaria ornata*. The percent cover of each category was calculated for each quadrat from 25 random points using the software PhotoQuad[73]. For each category, the percent cover corresponded to the number of points of that category divided by the total number of identifiable points in the quadrat. Data were then averaged per bommie across the 5 photographs.

Sample collection
After a 6-month acclimatation period, we sampled the BBL (~50 cm above the substrate) of each bommie, as well as the MBL (~5 cm above the substrate) of the substrate on each algal-removed bommie, and of substrates dominated by *T. ornata* or *D. bartayresiana* on each algal-dominated bommie (Fig. 1). Water samples were collected in duplicate to concurrently analyze both their microbiome and metabolome composition. Algal surfaces and whole tissues were collected for each algal species on each algal-dominated bommie for characterization of their metabolome and comparison with algal boundary layers. Sampling spanned over 9 days and was repeated four times: December 2020, March 2021, May 2021 & June 2021; except for whole tissues which were sampled once in February 2021.

BBL samples were collected using 10 L plastic pouches which were emptied of air and opened underwater generating a water inflow. MBL samples were collected using a modified version of the in-situ benthic chamber used by Kubanek et al. [74]. A 5 L bottom-less plastic bottle was placed over a patch of macroalgae (Supplementary Fig. 3). The top end of the bottle was connected to a hose leading to a manual bilge pump resting on the boat pouring the pumped water into a 10 L pouch. The inlet of the hose was at ~5 cm distance from the macroalgal thallus in the chamber. Water was then pumped during 10 min to obtain 7 L of seawater. To collect algal-removed MBL seawater, the same procedure was applied placing the chamber over a protruding substrate composed of a mix of bare substrate, CCA, thin (<5 mm) turf on algal-removed bommies (Supplementary Fig. 3b). Pouches were kept in a cool box with ice during transport (~15-20 min) back to the laboratory. For the collection of microbes, 5 L of seawater were pre-filtered with 47 mm glass filters (2.7 µm pore size, Grade GF/D, Whatman) and filtered on 47 mm polyethersulfone filters (0.2 µm pore size, Sigma). Filters were cut in small pieces with sterile tools and stored into 2 mL cryotubes tubes with 1 mL of DNA/RNA Shield (Zymo Research, USA). Samples were left overnight at room temperature and stored at −20 °C until DNA extraction. For metabolomics, 5 L of collected seawater were directly loaded onto Strata-XL solid-phase extraction (SPE) cartridges (2 g/20 mL, Phenomenex, USA), previously conditioned with 20 mL distilled water. Seawater samples were not acidified to extract a wide range of metabolites and avoid the preferential extraction of acidic metabolites. We used the Strata-XL sorbent, a large particle polymeric-based sorbent with a modified N-vinylpyrrolidone functional group, for its capacity to retain both polar and non-polar neutral analytes. Cartridges were fitted onto a vacuum manifold (Supelco) connected to a vacuum pump (Laboport N820,

KNF). After sample loading, cartridges were rinsed with 20 mL distilled water, dried on the vacuum manifold, lyophilized, and stored at −20 °C until elution. Cartridges of 2 g with loaded BBL and MBL samples were eluted with 13 mL 100% MeOH (HPLC-MS grade). MeOH were removed by evaporation with a Genevac centrifugal evaporator EZ-2 series (SP Industrie, Royaume-Uni), and extracts were stored at −20 °C until injection.

Algal thalli were collected in the vicinity of the algal-dominated bommies to avoid impacting the experimental treatment. Ten thalli of *Turbinaria ornata* and a single large patch of *Dictyota bartayresiana* (~ 20–25 cm side length) were collected during each of the four sampling periods. Immediately after collection, algae were placed into large zip bags filled with surrounding water and transported into a cool box back to the laboratory. Surface metabolites from each macroalga were extracted within 2 h following collection using a dipping method with MeOH as the extraction solvent[39]. Only healthy algal pieces with no biofouling or lesions were selected to avoid the extraction of non-algal and intracellular compounds. Extraction consisted in dipping algal pieces in a watch glass with 10 mL MeOH during 15 s for *Turbinaria* and 10 s for *Dictyota*[39]. Three successive extractions were performed with new algal material and the solvent was pooled into a 50 mL flask.

To sample algal whole tissue, we collected two 1 L zip bags per species in the vicinity of each algal-dominated bommie. On the boat, algae were rinsed several times (3–4 baths) with ambient seawater to remove sand, microfauna and epiphytes before being flash frozen into carbonic ice. Samples were lyophilized and stored at −20 °C until chemical extraction. Endometabolites were extracted from 250 mg of algal powder with a solvent mixture of methanol/dichloromethane (10 mL, v/v, 1:1). The methanol and dichloromethane were removed by evaporation with a Genevac centrifugal evaporator EZ-2 series (SP Industrie, Royaume-Uni). Samples were stored at −20 °C until injection. The sampling and extraction details are provided in the Supplementary Methods.

Extraction blanks ($n = 7$) were prepared for each sample type in parallel with samples to detect potential contaminants, from the pumping, tubing, plastic pouches, SPE resin, washing, elution, solvents, and remove these features from the data prior to analysis. For BBLs and MBLs, distilled water was used with the same protocols as for the biological samples. For algal surfaces and whole tissues, the preparation of blank samples was conducted without algal material.

Mass spectrometry analysis

Before injection, extracts were resolubilized with 100% MeOH (HPLC-MS grade) at a concentration of 0.5 mg/mL for whole tissue extracts and of 1 mg/mL for algal surface and water extracts. Due to distinct sample matrix composition, Quality Control (QC) samples were prepared for each sample type (i.e., whole tissue, surface and water) by pooling all respective samples at equimolar concentrations and equally divided into individual HPLC vials. Samples were injected over two analytical sequences to avoid analytical drift and computational limitation: (i) water extracts processed in MS1 full scan MS switching between positive and negative ionization modes, and (ii) algal whole tissue and surface extracts analyzed in full scan MS and data dependent MS2 in positive and negative ionization modes, separately. As water extracts could not be processed in MS2 due to budget constraints, a pooled sample of algal MBLs and BBLs was added to the 2nd sequence to retrieve fragmentation spectra from algal water samples during data processing. All samples were injected randomly to avoid systematic bias. Experimental blanks (i.e., $n = 4$ MeOH only for system suitability and $n = 7$ extraction blanks for contaminant detection) and QC samples were injected at the beginning and at the end of each analytical sequence to condition the column, assess carry-over effect, and detect contaminants. Additionally, QC of each sample type were injected every 8 samples to track analytical repeatability (Supplementary Fig. 13). Metabolomic profiles were acquired from 2 μL injection with a UHPLC system (Vanquish Thermo Scientific, MA, USA) coupled to a Q-Exactive Plus Orbitrap mass spectrometer (Thermo Scientific, MA, USA) with a HESI source. The chromatographic separation was carried out on a Luna Omega 1.6 μm Polar C18 column

100×2.1 mm (Phenomenex, Torrance, CA, USA) and consisted of H_2O + 1 ‰ formic acid (mobile phase A) and acetonitrile/isopropanol (50/50) + 1 ‰ formic acid (mobile phase B). A linear gradient was used with a flow rate of 0.250 mL/min: 0 to 2 min, at 2% B; 2 to 8 min, from 2 to 65% B; 8 to 25 min, from 65 to 100% B; 25 to 27 min, from 100 to 2% B, 27 to 31 min, at 2% B. Mass spectrometer settings were as follows: sheath, auxiliary and sweep gas 35, 10 and 0 AU, respectively; capillary voltage, 3500 V in positive mode and 2500 V in negative mode; capillary temperature, 320 °C; ESI probe heater temperature, 200 °C and S-lens RF level, 50. For the 1st sequence, full scan mass spectra (MS1) were acquired in both positive and negative ionization mode with a full scan MS window of 100–1500 m/z and a resolution of 35,000. The maximum injection time was set to 100 ms and automatic gain control (AGC) target set at 3.3×10^6. For the 2nd sequence, full scan MS resolution was set at 70,000 and MS/MS spectra were acquired in data dependent mode with an isolation window of 1.5 m/z; MS2 resolution 17 500; AGC target 3×10^5; maximum injection time 100 ms. Up to 5 of most intense selected ions per scan were fragmented with a stepped normalized collision energy of 25-35-45 eV. Dynamic exclusion was set to 5 s and isotope peaks were excluded.

Mass spectral data processing

Raw files were processed with MZmine 2 (2.53 version)[75] for MS extraction and features alignment. Please see the Supplementary Methods for the parameters used in MZmine 2. Two datasets were processed separately due to distinct MS acquisition modes and computational limitations. The 1st dataset included the samples from the five water types (MS1 data only; Supplementary Data 2) for characterization of their metabolomic signatures. The 2nd dataset included algal whole tissues, surfaces, and algal MBLs and BBLs (MS1 features and MS/MS fragmentation spectra; Supplementary Data 3) to further investigate the origin and diffusion of algal-derived metabolites.

MS1 peak intensities (i.e., peak areas) from each dataset were exported into a.csv file for statistical analysis. From the 2nd dataset with algal-associated features, we also exported a table comprising the peak intensities of MS1 features with MS2 data only as well as a.mgf file with consensus MS/MS spectra for network analysis and annotation purposes on the GNPS web platform[31] and SIRIUS software[25].

Quantitative tables of MS1 peak areas were imported and analyzed in the R environment and cleaned using an in-house R script. All analyses were performed on positive ionization mode data, except for the molecular subnetworks which were also investigated in negative ionization mode. Potential contaminants were removed from the data if their mean intensity in samples was less than 4 times their mean intensity in the blanks. Additionally, we filtered out low-quality features (i.e., D-ratio < 0.5 as defined in ref. [76]) and inconsistently detected features (i.e., present in less than 3 samples per sample type). The dataset with water samples (i.e., dataset 1) decreased from 14,131 MS1 features to 975 features after filtration (Supplementary Data 2). The dataset with the algal samples (i.e., dataset 2 in positive ionization mode) included 16,532 MS1 features, of which 4585 features with MS2 fragmentation spectra, and was reduced to 3943 MS1 features, of which 2214 with MS2, after filtration (Supplementary Data 3). In negative ionization mode, 1640 MS1 features had MS2 of which 1029 passed the filtration steps (Supplementary Data 5). MS1 peak intensities from water samples only (i.e., dataset 1; Supplementary Data 2) were log10 (x + 1) transformed. In the table with algal-associated MS1 features, each feature intensity was divided by the sum of intensities within each sample to control for the potential bias introduced by different sample injection concentrations. Relative intensities were then transformed by center-log ratio (CLR) with the addition of a constant equal to half the minimum value. Data were mean-centered for multivariate analysis.

Molecular networking and annotation strategy

Feature-Based Molecular Networks (FBMN) were built on GNPS[24] to connect molecular features based on their spectral similarity with a precursor ion mass tolerance of 0.02 Da, a cosine score of 0.7 and a minimum of

6 matched peaks. For each pair of nodes (i.e., molecular features), only the top 15 edges were kept. In addition, a search for analogs was defined with a maximum mass difference of 100 m/z from the mass of the precursor ion. We used an extended workflow via MolNetEnhancer[23] compiling Dereplicator[77], Network Annotation Propagation[78] and MS2LDA_MotifDB[79] in silico tools to retrieve their chemical classification (ClassyFire chemical ontology)[32] and improve annotations. Molecular networks were all visualized in Cytoscape[80].

To complete features dereplication, we used SIRIUS for putative molecular formulas and CANOPUS for compound class prediction[25,33]. MS2 m/z deviation was set to 5 ppm and a maximum of 10 potential results was considered. Molecular formulas were obtained considering all possible ionizations and without database search. The ZODIAC module was used to increase the confidence of putative formula[81] with parameters kept as default. We only considered proposed formulas with a ZODIAC score >0.95 and explaining at least 4 peaks and 85% of the spectral intensity. Comparing MolNetEnhancer and CANOPUS outputs allowed us to find a consensus at the class level. For most networks, both tools showed congruent results. When this was not the case, CANOPUS results were preferred when most compounds in the subnetwork belonged to the same class and if that class had a probability >0.9. If no consensus at the class level could be achieved, subnetworks were classified according to their superclass (e.g., lipids-like molecules) when possible, or categorized as "no consensus". Fatty acyls & glycerolipids were commonly found in the same networks, hence a mixed category was created. We manually verified the library hits of discussed networks and compared the putative formula given by SIRIUS using the MarinLit and Lipid maps online databases. Annotation results from GNPS and SIRIUS workflows are summarized in Supplementary Data 4 and 6 for the positive and negative ionization modes, respectively.

16S rDNA sequencing and metabarcoding data processing
DNA from water filters was extracted using the ZymoBIOMICS DNA Miniprep kit (Zymo Research, USA, D4300) according to manufacturer instructions for samples stored and lysed into DNA/RNA Shield. DNA extracts were then stored at −20 °C and dried with a centrifugal evaporator (EZ-2 series, Genevac) for shipping. Additionally, several blank extractions were performed for contaminant detection and removal (i.e., filters, extraction kits, Genevac & PCR). The hypervariable region V3-V4 of the 16S rDNA gene was amplified using the universal primers 341 F (5′-CCTACGGGNGGCWGCAG- 3′) and 805 R (3′-GACTACHVGGG-TATCTAATCC- 5′) suggested for marine bacteria and some archaea[82]. Amplicons were sequenced using an Illumina NovaSeq 6000 sequencer. Paired-end (2 × 250 pb) reads were processed using DADA2 on R[83] to infer ASVs (i.e., amplicon sequence variants). Reads with ambiguous N bases were discarded and primers were removed with the Cutadapt software[84]. Only sequences with a length of 200–250 pb and with a quality score superior to 2 or less than 3 expected errors were further processed for the estimation of the error rates. Sequences were denoised based on a modified error rate estimation function, by altering loess arguments (weights and span) and enforcing monotonicity, more suitable for NovaSeq data. After reads merging and ASVs inference, chimeric sequences and those detected in a single sample were removed. Taxonomy was assigned from phylum to genus levels using the Silva reference database (v138.1). The sequence table, taxa table and metadata were then imported in the *phyloseq* R package[85]. Data were filtered again by removing mitochondria and chloroplast ASVs, inconsistently detected ASVs across water types (i.e., at least 3 samples per water type) and contaminants with the *decontam* R package (prevalence method) using our blank samples. The 91 ASVs flagged as contaminants accounted for ~45% of the total reads, with some present in very high relative abundance (Supplementary Fig. 14). In contrast, inconsistently detected ASVs represented a minor fraction of the data, accounting for ~3% of the total reads and present in low relative abundance (Supplementary Fig. 13). To ensure that the removal of these ASVs did not alter data structure, we performed a Mantel test which showed a very high correlation between the initial and filtered matrices ($r^2 = 0.93$, $p < 0.001$, $nperm = 999$).

Processed and cleaned data resulted in 5517 ASVs and 12,693,811 reads (Supplementary Data 1). The library size was consistent across sample water types, except for one MBL sample (i.e., MBL-C5), which was discarded due to its low read number (Supplementary Table 1; Supplementary Fig. 15). For alpha-diversity measures (Shannon index), microbial counts were rarefed (rarefy_even_depth:*phyloseq* package[85]) based on the smallest library size (i.e., 145,538 reads). Beta-diversity analysis was performed on non-rarefied data and CLR-transformed abundance, with ASV agglomerated at the genus level due to the very high number of ASVs provided by NovaSeq.

Statistics and reproducibility
To investigate the influence of macroalgal assemblages on the chemical and microbial composition of waterscapes, randomly chosen coral bommies were used as experimental units ($n = 3$ algal-removed bommies and $n = 3$ algal-dominated bommies). On these bommies, we collected 5 water types ($n = 12$ samples per water type), and for algal-dominated bommies only, 2 algal surface samples and 2 algal whole tissue samples, with one from each of the two macroalgal species (i.e., *Turbinaria ornata* and *Dictyota bartayr-esiana*; $n = 12$ surface samples per algal species and $n = 3$ whole tissue samples per algal species). Sampling took place over four periods, beginning 6 months after the removal of macroalgae. Statistical analyses were performed in R version 4.2.3. Differences in benthic assemblages were assessed on Bray-Curtis dissimilarities of untransformed percent cover data by Permutational Multivariate Analysis of Variance (PERMANOVA, 999 permutations; adonis2:*vegan* package[86]) using (i) algal treatment (algal-dominated *vs.* algal-removal bommies) as fixed factor before removal of macroalgae, and (ii) algal treatment and month as fixed factors after the removal of macroalgae. Results were visualized using Principal Coordinate Analysis (PCoA).

Alpha-diversity (Shannon diversity index) of water microbiomes and metabolomes was calculated using rarefied microbiome count and MS1 feature log-transformed abundances, respectively. For each data type, alpha-diversity measures were compared between the 5 water types using one-way ANOVAs ($p < 0.05$), followed by post-hoc Tukey HSD tests. Assumptions of Gaussian distribution and homoscedasticity were verified with the *DHARMa* package[87]. Broad compositional differences in the microbiome and metabolome of sample types were tested by PERMANOVA and visualized by Principal Component Analysis (pca; *mixOmics* R package[88]).

To discriminate groups of samples and identify the ASVs and metabolites best differentiating these groups, we used partial least squares-discriminant analysis (PLS-DA; plsda:*mixOmics* R package[88]). Data was mean-centered, and the variability associated to repeated measures on bommies was accounted for with the argument "withinVariation". PLS-DAs were validated by cross-model validation (7-fold outer loop CV2 and 6-fold inner loop CV1), and the significance of the classification error rate (CER) was tested with a permutation test (999 permutations; *RVAideMe-moire* R package[89]). Two PLS-DAs were performed to discriminate between algal treatments within each boundary layer (i.e., horizontal comparisons): (i) BBL algal-removed *vs.* BBL algal-dominated samples and (ii) MBL algal-removed *vs.* MBL *Dictyota* *vs.* MBL *Turbinaria* samples. Two others were performed to discriminate between boundary layers within each algal treatment (i.e., vertical comparisons): (i) BBL algal-removed *vs.* MBL algal-removed samples and (ii) BBL algal-dominated *vs.* MBL *Dictyota* *vs.* MBL *Turbinaria* samples.

To explore whether the microbial and chemical (i.e., multi-omic) signatures were related, we integrated metabarcoding and MS1 metabolomic data using multiblock PLS-DA (DIABLO[30]; block.splsda:*mixOmics* R package[88]). DIABLO seeks for correlated variables between pair of datasets that also discriminate sample groups. Prior to run DIABLO, the level of association between the metabarcoding and metabolomic datasets was verified with a Mantel test ($p < 0.05$) on distance matrices and by the correlation of components obtained from PLS regression (correlation coefficient > 0.8). We set a weight of 1 for the association between datasets to favor the covariance between datasets over model's discriminative ability. The optimal number of components and variables were estimated by cross

validation using the function "tune.block.splsda". DIABLO outputs were validated by a permutation test based on cross-model validation.

To highlight the microbial genera that contributed most to the discrimination of the five water types, we used the Variable Importance in Projection (VIP) scores from PLS-DAs (VIP > 1) by summing the VIP scores of each variable across the four PLS-DA models. Heatmaps were used to represent the enrichment of the 50 top-ranked ASVs with the highest summed VIP scores in the different water types.

We performed an additional PLS-DA for each algal species to discriminate algal whole tissues, surfaces, MBLs, and algal-dominated BBL samples according to their metabolomic signatures and highlight features (MS1 with MS2 data) best discriminating sample types. These features were then used to identify molecular subnetworks of interest by selecting subnetworks comprising a minimum of 3 discriminant features (VIP > 1) and/or at least one feature with a VIP score superior to the median. Additionally, to highlight subnetworks of diffusing metabolites, only features detected in either or both whole tissue or surface and in the MBL were considered.

To investigate whether the diversity of diffusing metabolites across sample types varied with polarity, we analyzed the retention times of each feature weighted equally (i.e., unweighted retention times). Retention times in minutes were obtained from UHPLC reverse phase chromatography, where more polar features tend to be eluted first. In a second analysis, we accounted for feature abundance by weighting the retention times by the mean relative abundance of each feature within each sample type (i.e., abundance-weighted retention times). Due to violations of the homoscedasticity assumption, differences in abundance-weighted retention times across sample types were assessed using the non-parametric Kruskal-Wallis and post-hoc Dunn tests.

To further investigate covariations between ASVs and chemical features (MS1 with MS2 data) within the two algal MBLs, we conducted an additional DIABLO analysis. We focused on the algal MBLs, excluding the algal-dominated BBL, to reflect species-related changes and to avoid a confounding source of variation. Only previously identified discriminant ASVs ($n = 292$) and ion features ($n = 309$) were considered to specifically highlight the already discussed variables. Covariation patterns of highly positively (>0.7) and negatively (<0.7) correlated variables were represented as bipartite networks on Cytoscape[80].

Reporting summary
Further information on research design is available in the Nature Portfolio Reporting Summary linked to this article.

Data availability
Raw data and R scripts are accessible on Zenodo (https://doi.org/10.5281/zenodo.14366152). Metabarcoding sequence data have been deposited in the Sequence Read Archive under the accession code PRJNA941779. MS data are all publicly available in the Mass Spectrometry Interactive Virtual Environment (MassIVE) repository MSV000091424. FBMN workflows can be accessed in GNPS with the following links: https://gnps.ucsd.edu/ProteoSAFe/status.jsp?task=b9813b77629a4d44994e70febc96d82b; https://gnps.ucsd.edu/ProteoSAFe/status.jsp?task=55e170b22fd84e5ca890c75420566140; https://gnps.ucsd.edu/ProteoSAFe/status.jsp?task=8772ad1163da4a5eab30177b41e39722; https://gnps.ucsd.edu/ProteoSAFe/status.jsp?task=b0086676f483460bbb7f4d7a9b2145fe.

Code availability
R scripts to replicate the results are accessible on Zenodo (https://doi.org/10.5281/zenodo.14517147)[90].

References
1. Nelson, C. E., Wegley Kelly, L. & Haas, A. F. Microbial interactions with dissolved organic matter are central to coral reef ecosystem function and resilience. *Ann. Rev. Mar. Sci.* **15**, 431–460 (2023).
2. O'Neil, J. M. & Capone, D. G. Nitrogen cycling in coral reef environments. in *Nitrogen in the Marine Environment* (eds Capone, D. G., Bronk, D. A., Mulholland, M. R. & Carpenter, E. J.) 949–989 (Academic Press, 2008).
3. Silveira, C. B. et al. Microbial processes driving coral reef organic carbon flow. *FEMS Microbiol. Rev.* **41**, 575–595 (2017).
4. Nelson, C. E. et al. Coral and macroalgal exudates vary in neutral sugar composition and differentially enrich reef bacterioplankton lineages. *ISME J.* **7**, 962–979 (2013).
5. Wild, C. et al. Degradation and mineralization of coral mucus in reef environments. *Mar. Ecol. Prog. Ser.* **267**, 159–171 (2004).
6. Paul, V. J. et al. Chemically mediated interactions between macroalgae *Dictyota* spp. and multiple life-history stages of the coral *Porites astreoides*. *Mar. Ecol. Prog. Ser.* **426**, 161–170 (2011).
7. Wichard, T. & Beemelmanns, C. Role of chemical mediators in aquatic interactions across the Prokaryote–Eukaryote boundary. *J. Chem. Ecol.* **44**, 1008–1021 (2018).
8. Dennison, W. C. & Barnes, D. J. Effect of water motion on coral photosynthesis and calcification. *J. Exp. Mar. Biol. Ecol.* **115**, 67–77 (1988).
9. Weber, L. et al. Extracellular reef metabolites across the protected Jardines de la Reina Cuba Reef System. *Front Mar. Sci.* **7**, 1–17 (2020).
10. Walsh, K. et al. Aura-biomes are present in the water layer above coral reef benthic macro-organisms. *PeerJ* **5**, e3666 (2017).
11. Becker, C. C. et al. Microorganisms and dissolved metabolites distinguish Florida's Coral Reef habitats. *PNAS Nexus* **2**, 1–14 (2023).
12. Shashar, N., Kinane, S., Jokiel, P. L. & Patterson, M. R. Hydromechanical boundary layers over a coral reef. *J. Exp. Mar. Biol. Ecol.* **199**, 17–28 (1996).
13. Davis, K. A., Pawlak, G. & Monismith, S. G. Turbulence and coral reefs. *Ann. Rev. Mar. Sci.* **13**, 343–373 (2021).
14. Haas, A. F. et al. Global microbialization of coral reefs. *Nat. Microbiol.* **1**, 1–7 (2016).
15. Smith, J. E. et al. Re-evaluating the health of coral reef communities: baselines and evidence for human impacts across the central pacific. *Proc. R. Soc. B Biol. Sci.* **283**, 1–9 (2016).
16. Wegley Kelly, L. et al. Local genomic adaptation of coral reef-associated microbiomes to gradients of natural variability and anthropogenic stressors. *Proc. Natl. Acad. Sci. USA* **111**, 10227–10232 (2014).
17. Frade, P. R. et al. Spatial patterns of microbial communities across. *Commun. Biol.* **3**, 1–14 (2020).
18. Weber, L., Gonzalez-Díaz, P., Armenteros, M. & Apprill, A. The coral ecosphere: a unique coral reef habitat that fosters coral-microbial interactions. *Limnol. Oceanogr.* **64**, 2373–2388 (2019).
19. Weber, L. et al. Benthic exometabolites and their ecological significance on threatened Caribbean coral reefs. *ISME Commun.* **2**, 1–13 (2022).
20. Haas, A. F. et al. Effects of coral reef benthic primary producers on dissolved organic carbon and microbial activity. *PLoS ONE* **6**, e27973 (2011).
21. Wegley Kelly, L. et al. Distinguishing the molecular diversity, nutrient content, and energetic potential of exometabolomes produced by macroalgae and reef-building corals. *Proc. Natl. Acad. Sci. USA* **119**, 1–12 (2022).
22. Mannochio-russo, H. et al. Microbiomes and metabolomes of dominant coral reef primary producers illustrate a potential role for immunolipids in marine symbioses. *Commun. Biol.* **6**, 1–19 (2023).

23. Ernst, M. et al. Molnetenhancer: enhanced molecular networks by integrating metabolome mining and annotation tools. *Metabolites* **9**, 1–25 (2019).

24. Nothias, L. F. et al. Feature-based molecular networking in the GNPS analysis environment. *Nat. Methods* **17**, 905–908 (2020).

25. Dührkop, K. et al. SIRIUS 4: a rapid tool for turning tandem mass spectra into metabolite structure information. *Nat. Methods* **16**, 299–302 (2019).

26. Da Silva, R. R., Dorrestein, P. C. & Quinn, R. A. Illuminating the dark matter in metabolomics. *Proc. Natl. Acad. Sci. USA* **112**, 12549–12550 (2015).

27. Ochsenkühn, M. A., Schmitt-Kopplin, P., Harir, M. & Amin, S. A. Coral metabolite gradients affect microbial community structures and act as a disease cue. *Commun. Biol.* **1**, 1–10 (2018).

28. Barott, K. L. & Rohwer, F. L. Unseen players shape benthic competition on coral reefs. *Trends Microbiol.* **20**, 621–628 (2012).

29. Jorissen, H. et al. Evidence for water-mediated mechanisms in coral–algal interactions. *Proc. R. Soc. B Biol. Sci.* **283**, 1–10 (2016).

30. Singh, A. et al. DIABLO: an integrative approach for identifying key molecular drivers from multi-omics assays. *Bioinformatics* **35**, 3055–3062 (2019).

31. Wang, M. et al. Sharing and community curation of mass spectrometry data with Global Natural Products Social Molecular Networking. *Nat. Biotechnol.* **34**, 828–837 (2016).

32. Feunang, Y. D. et al. ClassyFire: automated chemical classification with a comprehensive, computable taxonomy. *J. Cheminform.* **8**, 1–20 (2016).

33. Dührkop, K. et al. Systematic classification of unknown metabolites using high-resolution fragmentation mass spectra. *Nat. Biotechnol.* **39**, 462–471 (2021).

34. Takikawa, M. et al. Crenulacetal C, a marine diterpene, and its synthetic mimics inhibiting Polydora websterii, a harmful lugworm damaging pearl cultivation. *Chem. Pharm. Bull.* **46**, 462–466 (1998).

35. Schmitt, T. M., Lindquist, N. & Hay, M. E. Seaweed secondary metabolites as antifoulants: effects of Dictyota spp. diterpenes on survivorship, settlement, and development of marine invertebrate larvae. *Chemoecology* **8**, 125–131 (1998).

36. Seymour, J. R., Brumley, D. R., Stocker, R. & Raina, J. B. Swimming towards each other: the role of chemotaxis in bacterial interactions. *Trends Microbiol* **32**, 640–649 (2024).

37. Silveira, C. B. et al. Bacterial community associated with the reef coral *Mussismilia braziliensis*'s momentum boundary layer over a diel cycle. *Front. Microbiol.* **8**, 1–12 (2017).

38. Ghisalberti, M. & Nepf, H. The structure of the shear layer in flows over rigid and flexible canopies. *Environ. Fluid Mech.* **6**, 277–301 (2006).

39. Othmani, A., Briand, J. F., Ayé, M., Molmeret, M. & Culioli, G. Surface metabolites of the brown alga *Taonia atomaria* have the ability to regulate epibiosis. *Biofouling* **32**, 801–813 (2016).

40. Lachnit, T., Fischer, M., Künzel, S., Baines, J. F. & Harder, T. Compounds associated with algal surfaces mediate epiphytic colonization of the marine macroalga *Fucus vesiculosus*. *FEMS Microbiol. Ecol.* **84**, 411–420 (2013).

41. Slattery, M. & Lesser, M. P. Allelopathy in the tropical alga *Lobophora variegata* (Phaeophyceae): mechanistic basis for a phase shift on mesophotic coral reefs? *J. Phycol.* **50**, 493–505 (2014).

42. Rasher, D. B., Stout, E. P., Engel, S., Kubanek, J. & Hay, M. E. Macroalgal terpenes function as allelopathic agents against reef corals. *Proc. Natl. Acad. Sci. USA* **108**, 17726–17731 (2011).

43. Barbosa, J. P., Teixeira, V. L. & Pereira, R. C. A dolabellane diterpene from the brown alga *Dictyota pfaffii* as chemical defense against herbivores. *Botanica Mar.* **47**, 147–151 (2004).

44. Chen, J. et al. Diterpenes from the marine algae of the genus *Dictyota*. *Mar. Drugs* **16**, 1–25 (2018).

45. Zuo, Z. Why algae release volatile organic compounds—the emission and roles. *Front. Microbiol.* **10**, 1–7 (2019).

46. Cárdenas, A. et al. Excess labile carbon promotes the expression of virulence factors in coral reef bacterioplankton. *ISME J.* **12**, 59–76 (2018).

47. Heringdorf, Dagmar. M. Z. Lysophospholipids. in *Encyclopedia of Molecular Pharmacology* (eds Offermanns, S. & Rosenthal, W.) 710–716 (Springer, 2008).

48. Teramoto, M. et al. *Oleibacter marinus* gen. nov., sp. nov., a bacterium that degrades petroleum aliphatic hydrocarbons in a tropical marine environment. *Int. J. Syst. Evol. Microbiol.* **61**, 375–380 (2011).

49. Gómez-Pereira, P. R. et al. Genomic content of uncultured Bacteroidetes from contrasting oceanic provinces in the North Atlantic Ocean. *Environ. Microbiol.* **14**, 52–66 (2012).

50. McCarren, J. et al. Microbial community transcriptomes reveal microbes and metabolic pathways associated with dissolved organic matter turnover in the sea. *Proc. Natl. Acad. Sci. USA* **107**, 16420–16427 (2010).

51. Jung, M. Y. et al. *Hoeflea halophila* sp. nov., a novel bacterium isolated from marine sediment of the East Sea, Korea. *Antonie van. Leeuwenhoek* **103**, 971–978 (2013).

52. Wu, Y. H. et al. *Croceicoccus pelagius* sp. nov. and *Croceicoccus mobilis* sp. nov., isolated from marine environments. *Int. J. Syst. Evol. Microbiol.* **66**, 4506–4511 (2016).

53. Clerc, E. E. et al. Strong chemotaxis by marine bacteria towards polysaccharides is enhanced by the abundant organosulfur compound DMSP. *Nat. Commun.* **14**, 1–14 (2023).

54. Tout, J. et al. Chemotaxis by natural populations of coral reef bacteria. *ISME J.* **9**, 1764–1777 (2015).

55. Zaneveld, J. R. et al. Overfishing and nutrient pollution interact with temperature to disrupt coral reefs down to microbial scales. *Nat. Commun.* **7**, 1–12 (2016).

56. Ziegler, M. et al. Coral microbial community dynamics in response to anthropogenic impacts near a major city in the central Red Sea. *Mar. Pollut. Bull.* **105**, 629–640 (2016).

57. Frias-Lopez, J., Zerkle, A. L., Bonheyo, G. T. & Fouke, B. W. Partitioning of bacterial communities between seawater and healthy, black band diseased and dead coral surfaces. *Appl. Environ. Microbiol.* **68**, 2114–2228 (2002).

58. MacKnight, N. J. et al. Microbial dysbiosis reflects disease resistance in diverse coral species. *Commun. Biol.* **4**, 1–11 (2021).

59. Wang, G. et al. Phylogenetic analysis of epiphytic marine bacteria on Hole-Rotten diseased sporophytes of *Laminaria japonica*. *J. Appl. Phycol.* **20**, 403–409 (2008).

60. Fernandes, N. et al. Genomes and virulence factors of novel bacterial pathogens causing bleaching disease in the marine red alga *Delisea pulchra*. *PLoS ONE* **6**, e27387 (2011).

61. Rosado, P. M. et al. Marine probiotics: increasing coral resistance to bleaching through microbiome manipulation. *ISME J.* **13**, 921–936 (2019).

62. Zhang, Y. et al. Shifting the microbiome of a coral holobiont and improving host physiology by inoculation with a potentially beneficial bacterial consortium. *BMC Microbiol.* **21**, 1–14 (2021).

63. Maire, J. et al. Intracellular bacteria are common and taxonomically diverse in cultured and in hospite algal endosymbionts of coral reefs. *ISME J.* **15**, 2028–2042 (2021).

64. Raina, J. B., Dinsdale, E. A., Willis, B. L. & Bourne, D. G. Do the organic sulfur compounds DMSP and DMS drive coral microbial associations? *Trends Microbiol.* **18**, 101–108 (2010).

65. Fernandez, E., Ostrowski, M., Siboni, N., Seymour, J. R. & Petrou, K. Uptake of dimethylsulfoniopropionate (DMSP) by natural microbial communities of the Great Barrier Reef (GBR), Australia. *Microorganisms* **9**, 1–23 (2021).

66. Liu, J. et al. Bacterial dimethylsulfoniopropionate biosynthesis in the East China Sea. *Microorganisms* **9**, 1–22 (2021).

67. Cai, L. et al. Exploring coral microbiome assemblages in the South China Sea. *Sci. Rep.* **8**, 1–13 (2018).

68. Furukawa, T. et al. Inhibitory effect of sulfoquinovosyl diacylglycerol on prokaryotic DNA polymerase I activity and cell growth of *Escherichia coli*. *J. Oleo Sci.* **56**, 43–47 (2007).

69. Gomes, L. et al. Seaweeds' pigments and phenolic compounds with antimicrobial potential. *Biomol. Concepts* **13**, 89–102 (2022).

70. Pereira, R. C. et al. Associational defense against herbivory between brown seaweeds. *Phycologia* **49**, 424–428 (2010).

71. Yang, L., Tan, R. X., Wang, Q., Huang, W. Y. & Yin, Y. X. Antifungal cyclopeptides from *Halobacillus litoralis YS3106* of marine origin. *Tetrahedron Lett.* **43**, 6545–6548 (2002).

72. Dworjanyn, S. A., De Nys, R. & Steinberg, P. D. Localisation and surface quantification of secondary metabolites in the red alga *Delisea pulchra*. *Mar. Biol.* **133**, 727–736 (1999).

73. Trygonis, V. & Sini, M. PhotoQuad: A dedicated seabed image processing software, and a comparative error analysis of four photoquadrat methods. *J. Exp. Mar. Biol. Ecol.* **424–425**, 99–108 (2012).

74. Kubanek, J. et al. Multiple defensive roles for triterpene glycosides from two Caribbean sponges. *Oecologia* **131**, 125–136 (2002).

75. Pluskal, T., Castillo, S., Villar-Briones, A. & Orešič, M. MZmine 2: Modular framework for processing, visualizing, and analyzing mass spectrometry-based molecular profile data. *BMC Bioinform.* **11**, 1–11 (2010).

76. Broadhurst, D. et al. Guidelines and considerations for the use of system suitability and quality control samples in mass spectrometry assays applied in untargeted clinical metabolomic studies. *Metabolomics* **14**, 1–17 (2018).

77. Mohimani, H. et al. Dereplication of peptidic natural products through database search of mass spectra. *Nat. Chem. Biol.* **13**, 30–37 (2017).

78. Da Silva, R. R. et al. Propagating annotations of molecular networks using in silico fragmentation. *PLoS Comput. Biol.* **14**, 1–26 (2018).

79. Van der Hooft, J. J. J., Wandy, J., Barrett, M. P., Burgess, K. E. V. & Rogers, S. Topic modeling for untargeted substructure exploration in metabolomics. *Proc. Natl. Acad. Sci. USA* **113**, 13738–13743 (2016).

80. Shannon, P. et al. Cytoscape: a software environment for integrated models. *Genome Res.* **13**, 426 (2003).

81. Ludwig, M. et al. Database-independent molecular formula annotation using Gibbs sampling through ZODIAC. *Nat. Mach. Intell.* **2**, 629–641 (2020).

82. Klindworth, A. et al. Evaluation of general 16S ribosomal RNA gene PCR primers for classical and next-generation sequencing-based diversity studies. *Nucleic Acids Res.* **41**, 1–11 (2013).

83. Callahan, B. J. et al. DADA2: High-resolution sample inference from Illumina amplicon data. *Nat. Methods* **13**, 581–583 (2016).

84. Martin, M. Cutadapt removes adapter sequences from high throughput sequencing reads. *EMBnet J.* **17**, 10–12 (2011).

85. McMurdie, P. J. & Holmes, S. phyloseq: An R package for reproducible interactive analysis and graphics of microbiome census data. *PLoS ONE* **8**, e61217 (2013).

86. Oksanen, A. J. et al. vegan: Community Ecology package. R package version 2.6.4. (2022).

87. Hartig F. DHARMa: Residual Diagnostics for Hierarchical (Multi-Level / Mixed) Regression Models. R package version 0.4.6. (2022).

88. Rohart, F., Gautier, B., Singh, A. & Lê Cao, K. A. mixOmics: An R package for 'omics feature selection and multiple data integration. *PLoS Comput Biol.* **13**, 1–19 (2017).

89. Hervé, M. R. Package 'RVAideMemoire': Testing and Plotting Procedures for Biostatistics. (2023).

90. Pozas-Schacre, C. et al. Invasive macroalgae shape chemical and microbial waterscapes on coral reefs [Data set]. Zenodo. https://doi.org/10.5281/zenodo.14517147 (2024).

Author contributions
C.P.S and M.M.N designed the research. C.P.S and H.B performed the experiment. C.P.S, D.R and I.B carried out the microbial and chemical lab work. C.P.S and I.B analyzed the data. D.R, S.C, C.C, I.B and M.M.N contributed to instrumentalization and analytical tools. C.P.S and M.M.N drafted the manuscript. All authors contributed to revisions thereafter and gave final approval for submission.

Competing interests
The authors declare no competing interest.

Additional information
Supplementary information The online version contains supplementary material available at https://doi.org/10.1038/s42003-024-07433-6.

Correspondence and requests for materials should be addressed to Chloé. Pozas-Schacre.

Peer review information *Communications Biology* thanks Craig Nelson and the other, anonymous, reviewer(s) for their contribution to the peer review of this work. Primary Handling Editors: Linn Hoffmann and Tobias Goris.

Reprints and permissions information is available at http://www.nature.com/reprints

Publisher's note Springer Nature remains neutral with regard to jurisdictional claims in published maps and institutional affiliations.